UNITED STATES DEPARTMENT OF THE INTERIOR

GEOLOGICAL SURVEY

GEOLOGY OF THE IGNEOUS COMPLEX AT TINCUP PEAK, KALMIOPSIS WILDERNESS AREA, SOUTHWESTERN OREGON

By

Floyd Gray

U.S. Geological Survey
Open-File Report 80-1243
1980

Table of Contents

Illustrations

Tables

GEOLOGY OF THE IGNEOUS COMPLEX AT TINCUP PEAK, KALMIOPSIS WILDERNESS AREA, SOUTHWESTERN OREGON

By

Floyd Gray

ABSTRACT

The Late Jurassic mafic-ultramafic complex at Tincup Peak, southwestern Oregon, consists of two cumulate rock series, wehrlitic and lherzolitic, formed by fractional crystallization of two geochemically distinct batches of magma. The wehrlitic series forms a sill-like body that was emplaced into layered lherzolitic series rocks causing subsequent fracturing along contact margins. The two rock series are unrelated genetically but spatially linked due to multiple intrusion along a crustal weakness.

The lherzolitic series consists of the rock sequence: dunite-lherzolite, olivine-clinopyroxene heteradcumulate, olivine-bronzite cumulate and two-pyroxene gabbro, generated by the sequential crystallization of olivine, clinopyroxene, orthopyroxene, and plagioclase. Lherzolitic series rocks resemble those of tholeiitic stratiform intrusions, although the rocks are part of a dismembered ophiolite. Rocks from the wehrlitic series at Tincup Peak include wehrlite, olivine clinopyroxenite, magnetite clinopyroxenite, magnetite-hornblende clinopyroxenite, and hornblende gabbro resulting from the crystallization sequence: olivine$\pm$clinopyroxene, magnetite, hornblende, and plagioclase. Vanadium-rich cumulus magnetite, displaying graded bedding and forming discrete magnetite layers, occurs in zones in the wehrlitic series. The wehrlitic series seems to be similar in mineralogy and chemistry to the zoned ultramafic complexes with alkaline affinities of southeastern Alaska.

INTRODUCTION

Geologic setting

The Tincup Peak igneous complex forms part of an arcuate belt of mafic and ultramafic rocks within the western Jurassic belt in northern California and southwestern Oregon (figs. 1, 2). The crystalline rocks of the western Jurassic belt are composed mainly of ultramafic and gabbroic to dioritic rocks that are part of westward-overriding thrust sheets (fig. 3). Based on reconnaisance mapping at a scale of 1:62,500, the area adjacent to Tincup Peak has been subdivided into four parts, described as follows: (1) The northern part, including the area mapped in detail for this project, contains a north- to northeast-trending igneous complex consisting predominantly of gabbro, diorite, and metagabbro with lesser amounts of ultramafic rocks (Bailey and others, 1970; Blake and others, 1967; Blake, 1969). Further to the north, Hotz (1971) has dated quartz diorite of this part of the belt at 150 m.y. and called the assemblage the Chetco River Complex, which does not include ultramafic and metamorphosed amphibolitic rocks found within the area. (2) The western part is composed of the Dothan Formation over which the Chetco River igneous complex and the Josephine ultramafic sheet have been transported (Baldwin, 1969). The Dothan Formation is an Upper Jurassic (Ramp, 1969, 1975) to Lower Cretaceous (W. N. Blair, written commun., 1978) wedge of flysch

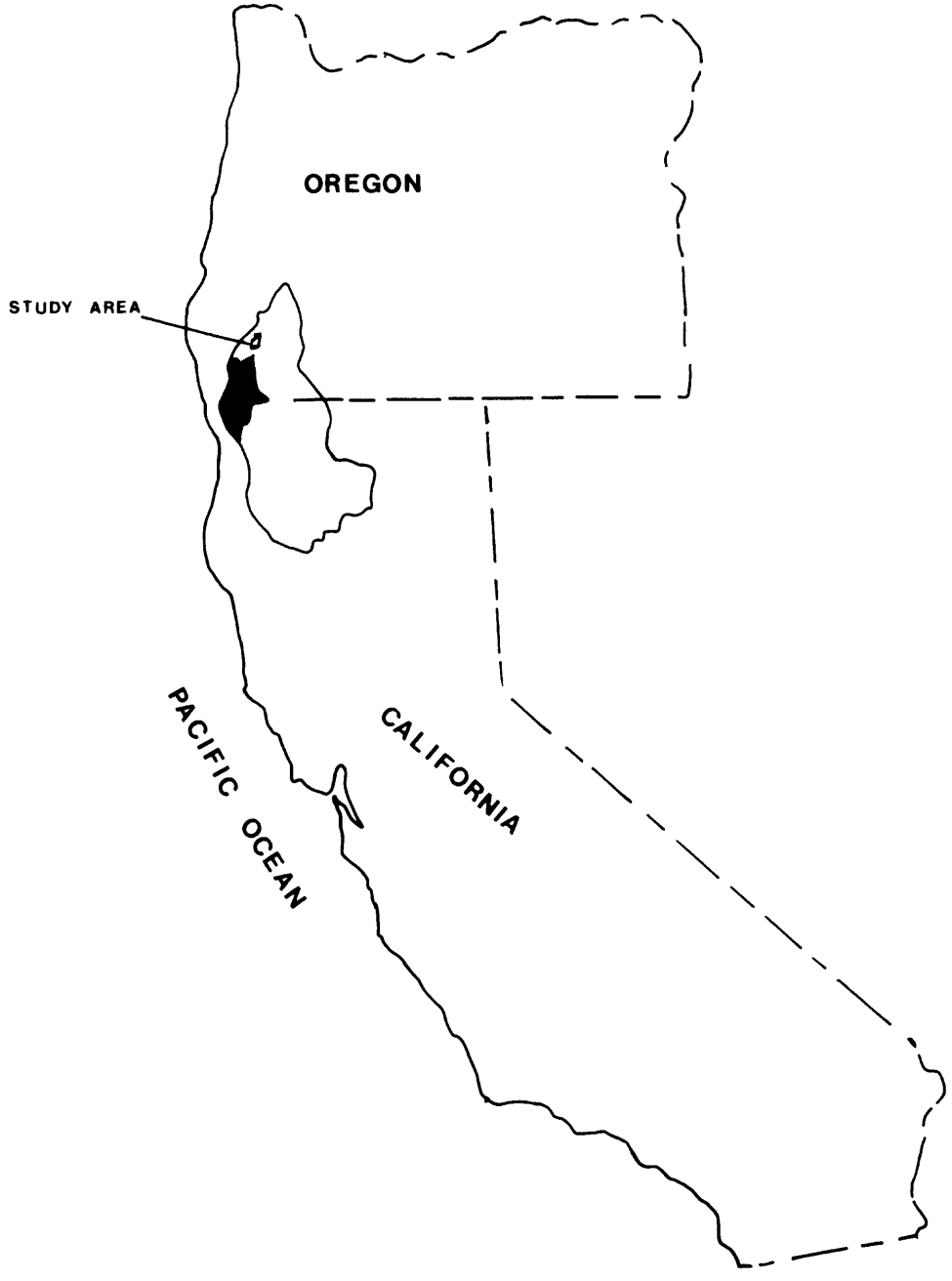

Figure 1.--Index map showing location of study area and its proximity to the Josephine ultramafic complex (black) in the Klamath Mountain geologic province.

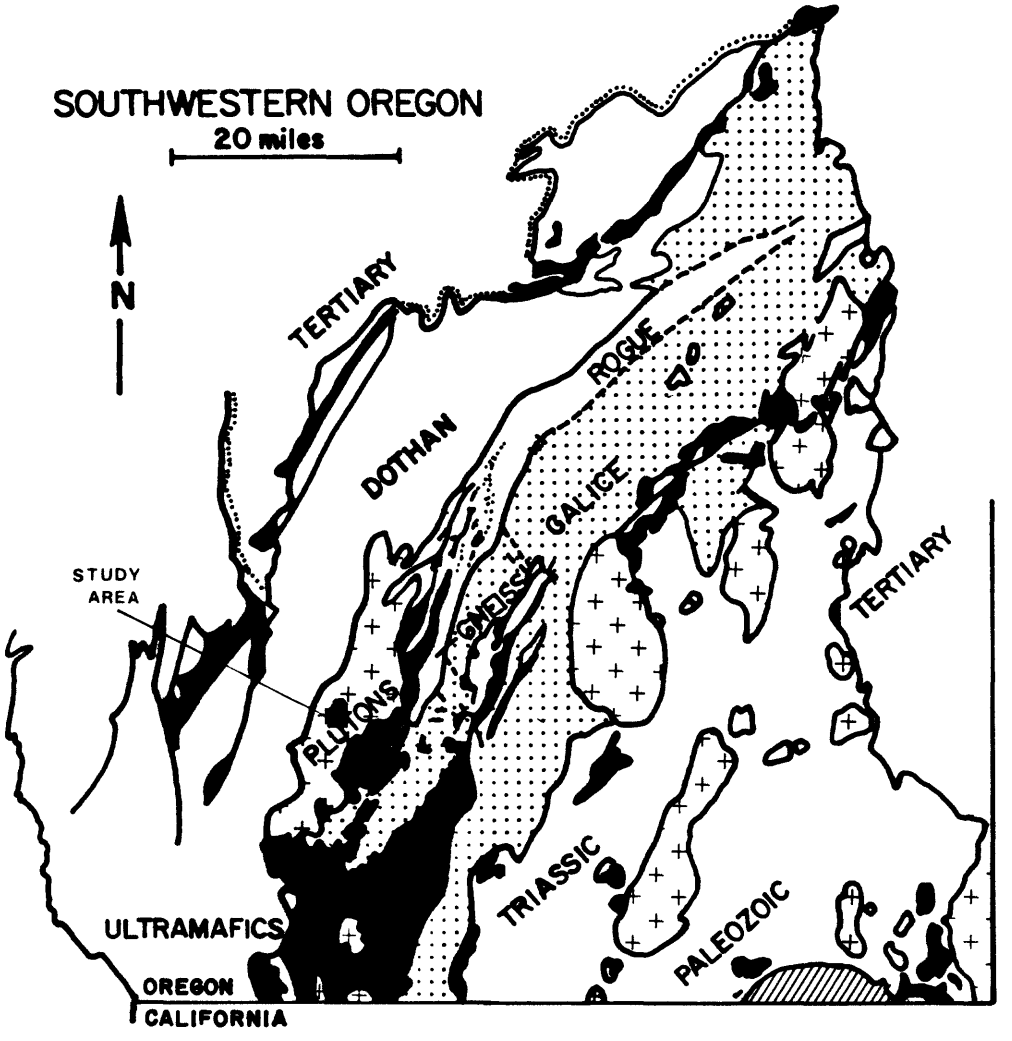

Figure 2.--Generalized regional geologic map of part of southwestern Oregon showing boundaries and trends of the lithic belts of pre-Tertiary Klamath Mountains. Modified from Wells and Peck (1961).

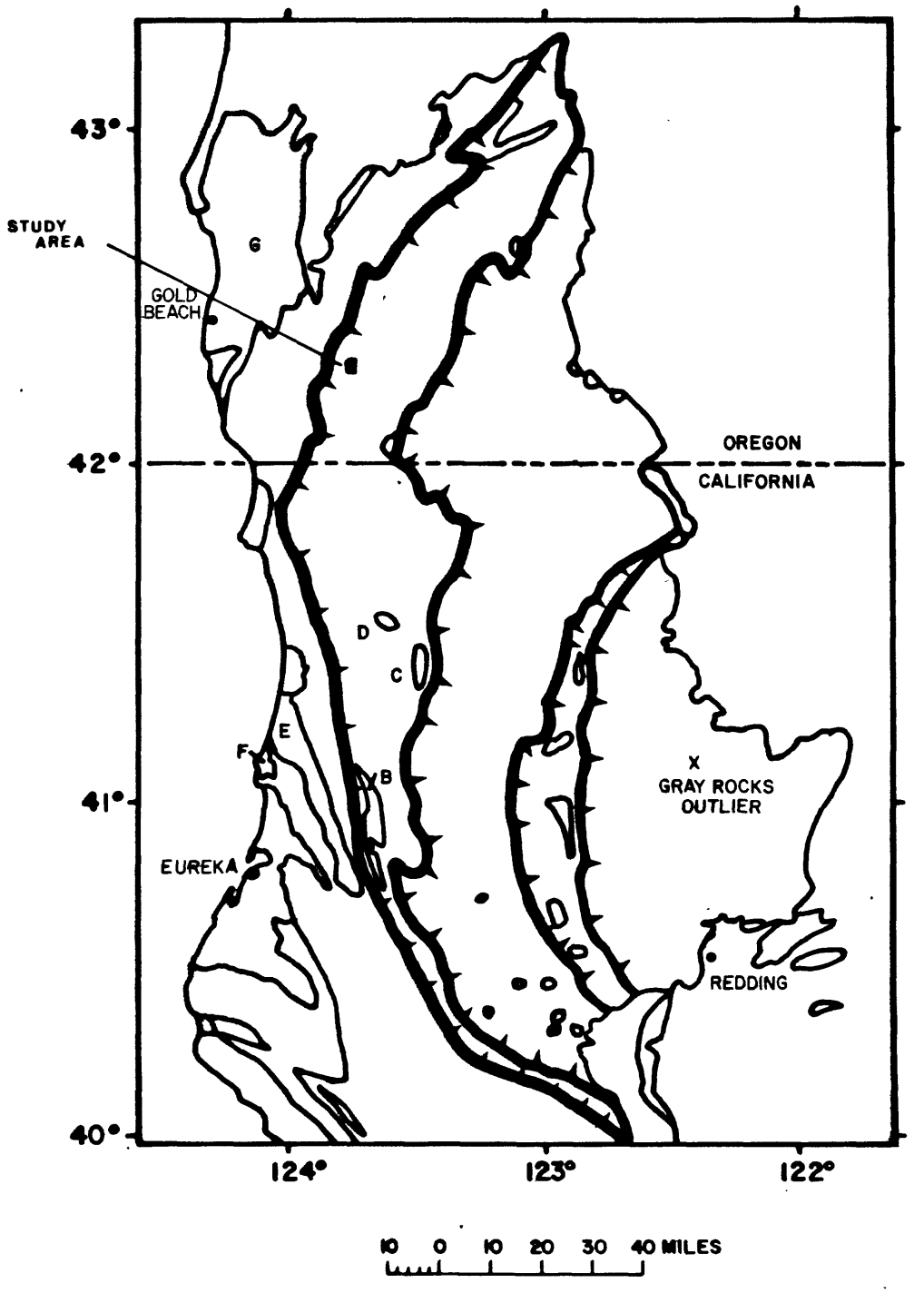

Figure 3.--Map showing principal postulated thrust plates in the Klamath Mountains. Modified from Irwin (1966).

sediments locally interlayered with irregular tabular bodies of altered basalt and minor chert. (3) The eastern portion of the area has been mapped (Page and others, 1980) as a melange sequence with folded sedimentary and volcanic rocks of uncertain age interspersed with serpentinite slices, and amphibolitic and dioritic rocks. (4) The southern part consists of the Josephine ultramafic complex composed of harzburgite with dunite and lherzolite thrust northward over the Chetco River Complex (Dick, 1976; Ramp, 1975; Medaris and Dott, 1970; Dott, 1965; Irwin, 1964).

Previous research

The Tincup Peak area has not previously been investigated in detail (Diller, 1902, 1914; Diller and Kay, 1924; Medaris and Dott, 1970; Ramp, 1957, 1961, 1972; Walker, 1973; Wells and others, 1949; Wells, 1955). In the Dry Butte terrane, a geologically similar region about 7 mi due south of Tincup Peak, Loney and Himmelberg (1977) considered amphibolitic rocks as the oldest rocks. These rocks have undergone regional metamorphism to the amphibolite facies and three episodes of folding. Partially recrystallized ultramafic rocks structurally overlie the amphibolite, show a less complex fold geometry, and display relic textures that suggest accumulation from a magma. Both the amphibolite and the ultramafic rocks were intruded by hornblende gabbro. Subsequently, a final deformational episode affected all three units. Intrusion of the hornblende gabbro was probably contemporaneous with the second (middle) period of deformation and continued intermittently to the final stages of the third and final deformational period. The authors suggest that although the Dry Butte terrane lacks a well-developed cumulate gabbro zone, the proximity of the alpine-type Josephine ultramafic complex with the other rocks of the Dry Butte terrane suggests a basal ultramafic tectonite complex and part of the gabbroic complex of an ophiolite sequence.

Accessiblity

The Tincup Peak area in Josephine County, southwestern Oregon, is located in the northern portion of the Kalmiopsis Wilderness Area and has very limited access (fig. 4). East of the Wilderness area, the Selma access road branches off of the Redwood Highway (State Highway 199) at Selma. This road turns into a four-wheel-drive track after it intersects the Illinois River at McCaleb Ranch, and ends at the Wilderness boundary at Chetco Pass. From there the Gold Basin Trail, approximately 7.5 mi, leads directly into the Tincup area. Two other roads, originating at Brookings to the west and Kerby to the east, lead to the Wilderness boundary but are not the most direct routes to the Tincup Peak area.

Rock names

The terminology used here follows that of the IUGS subcommission on the systematics of igneous rocks (fig. 5) from Streckeisen (1973).

Acknowledgments

I would like to extend my deepest gratitude to Dr. Norman J Page of the U.S. Geological Survey who introduced me to the ophiolites of southwestern Oregon, and continued to provide helpful insights throughout the research and writing of this thesis. I am also indebted to S. A. Morse for numerous

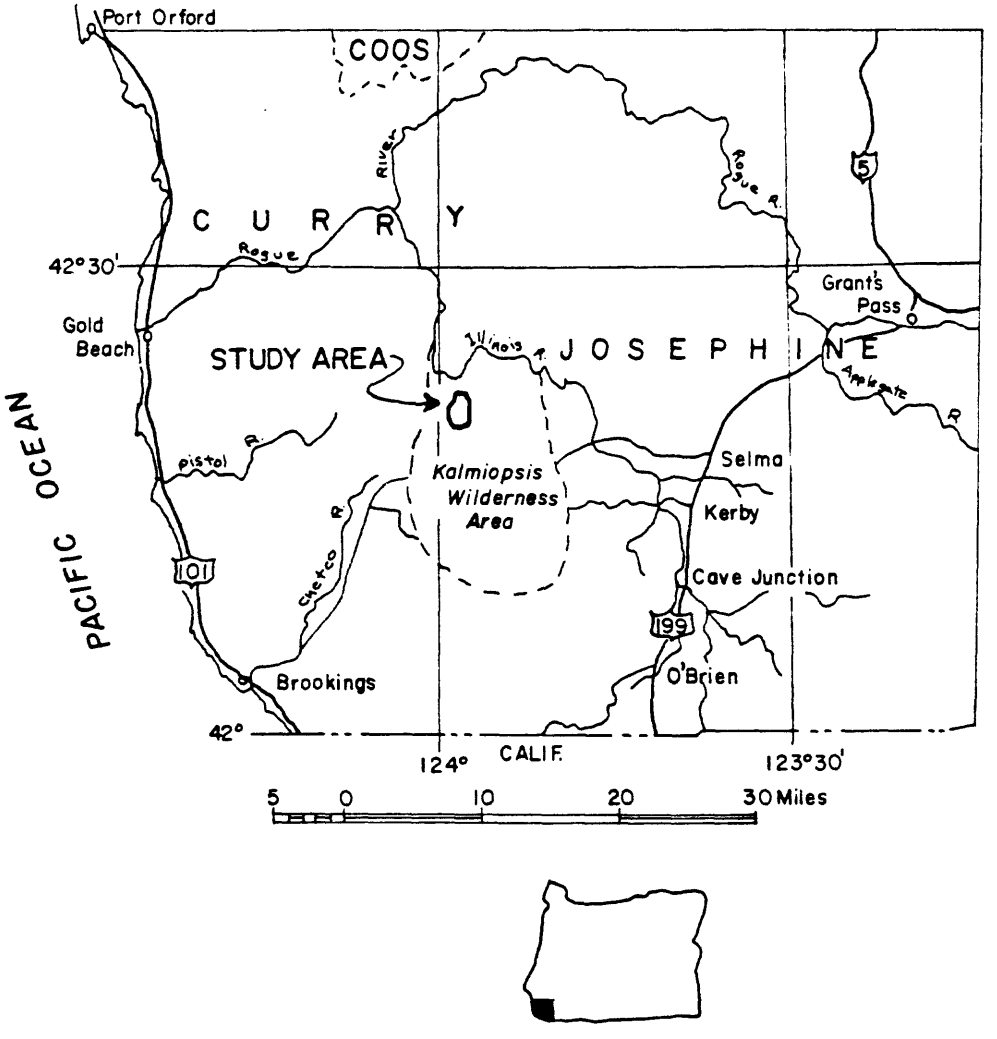

Figure 4.--Sketch map of southwestern Oregon showing major access routes into the Kalmiopsis Wilderness area.

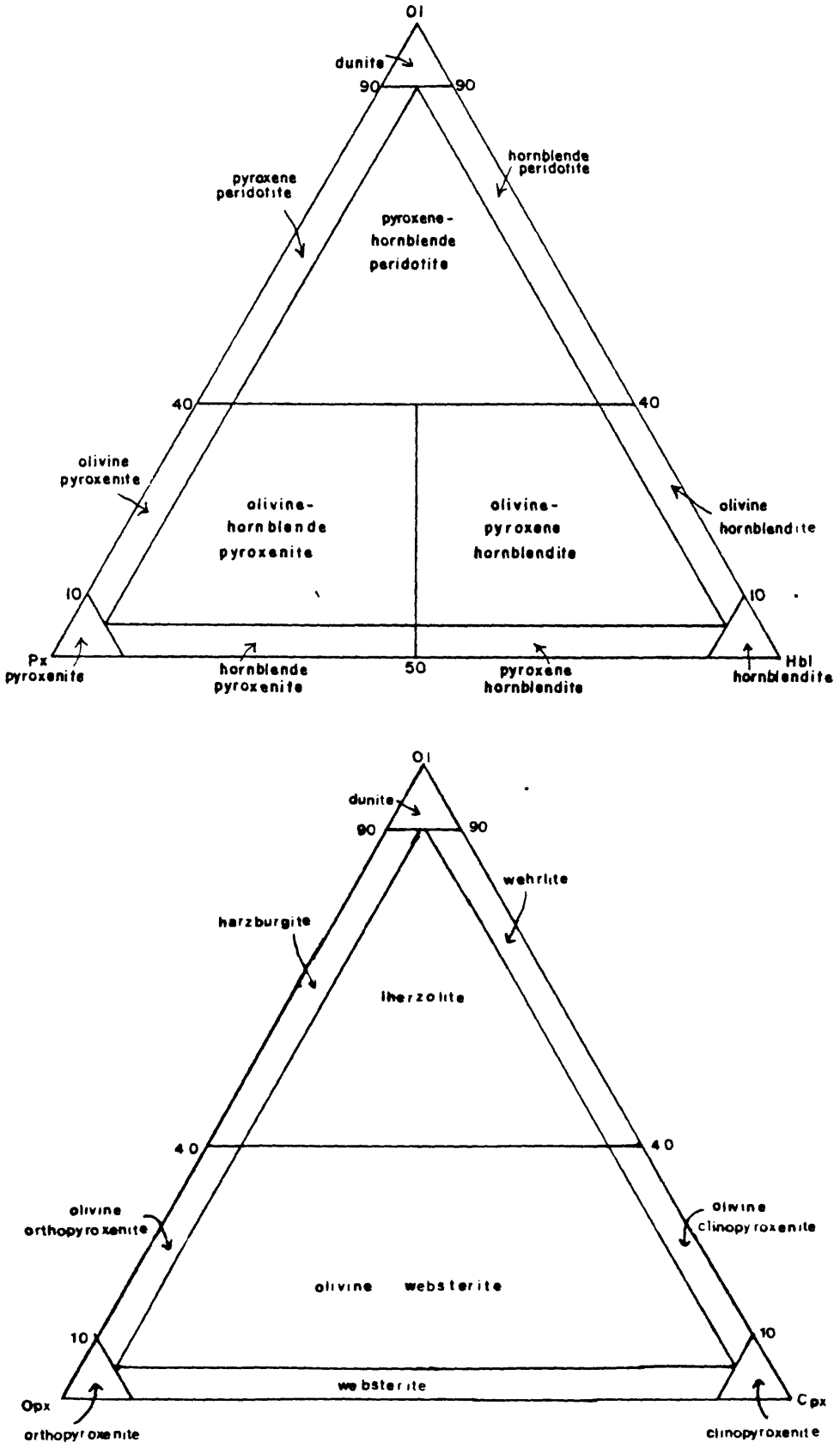

Figure 5.--Classification of ultramafic rocks with and without hornblende after Strieckeisen (1973), based on the relative percentages of olivine (Ol), orthopyroxene (Opx), clinopyroxene (Cpx), and ± hornblende (Hbl).

discussions that helped clarify my thinking and occasionally redirect my efforts toward more fundamental problems. Critical reviews of the manuscript by S. E. Haggerty and Peter Robinson are gratefully acknowledged. Special thanks go to W. A. Ranson, Joel Sparks, and Brendon McMahon for help in times of trouble. L. A. Page served as field assistant and trail blazer. Semiquantitative analyses were made by David Grimes of the U.S. Geological Survey, Denver office. Laboratory work was partially supported by a Sigma Xi grant-in-aid of research.

A special thanks must also be extended to my wife, Victoria, whose patience and encouragement were without exception throughout the duration of this project.

GENERAL GEOLOGIC DESCRIPTION

The Tincup Peak igneous complex of Jurassic age is a lenticular fault-bounded series of ultramafic and mafic rock that crops out in an area approximately 7 km long and 3 km wide in the northwestern Klamath Mountains of Oregon (fig. 6, map in pocket) The complex is bordered to the south and west by Late Jurassic to Cretaceous foliated hornblende gabbro intrusive rocks whose contact with the ultramafic rocks crops out mainly along a shallow east-northeast-dipping fault. Locally, the foliated hornblende gabbro crosscuts the trend of the contact and intrudes the ultramafic block. To the north, the ultramafic rocks pinch out in a complex manner and gabbro becomes the dominant rock type. In the east, fresh gabbro dips beneath an erosional surface of Tertiary gravels at the edge of the map area.

Although the ultramafic-mafic block is emplaced by faulting to its present position, the nature of the exposed rocks suggests that one group of ultramafics, the lherzolitic series, crystallized in a quiescent horizontal condition. A later wehrlitic series was intruded in the area and in part shows evidence of cumulus crystallization. The two groups of rocks are separated in the field on the basis of mineralogy and texture.

Ultramafic rocks

The distribution of ultramafic rocks is shown in figure 6. Ultramafic rocks consist of a lherzolitic series and a wehrlitic series. The lherzolitic series consists of dunites with thin chromitite layers, lherzolites, olivine-clinopyroxene heteradcumulates, and plagioclase-bearing peridotites composed of cumulus olivine and orthopyroxene crystals with poikilitic clinopyroxene. The wehrlitic series consists of wehrlite, olivine clinopyroxenite, magnetite clinopyroxenite, and a plagioclase-bearing hornblende magnetite clinopyroxenite (fig. 7). Contacts between the two units are in most places obscured by serpentinization, shearing along compositional boundaries, and late intrusion of mafic magmas accompanied by hydrothermal solutions.

Both groups of ultramafic rocks display a wide range of textures characteristic of cumulus crystallization, tectonic recrystallization and metamorphism, and partial recrystallization by thermal metamorphism associated with intrusion of later mafic rock types.

The predominant primary minerals found in these rocks are olivine, diopside, orthopyroxene, spinel, plagioclase, and green hornblende. Secondary minerals are ubiquitous and include green hornblende, serpentine group minerals, magnetite, talc, epidote, actinolite, and chlorite.

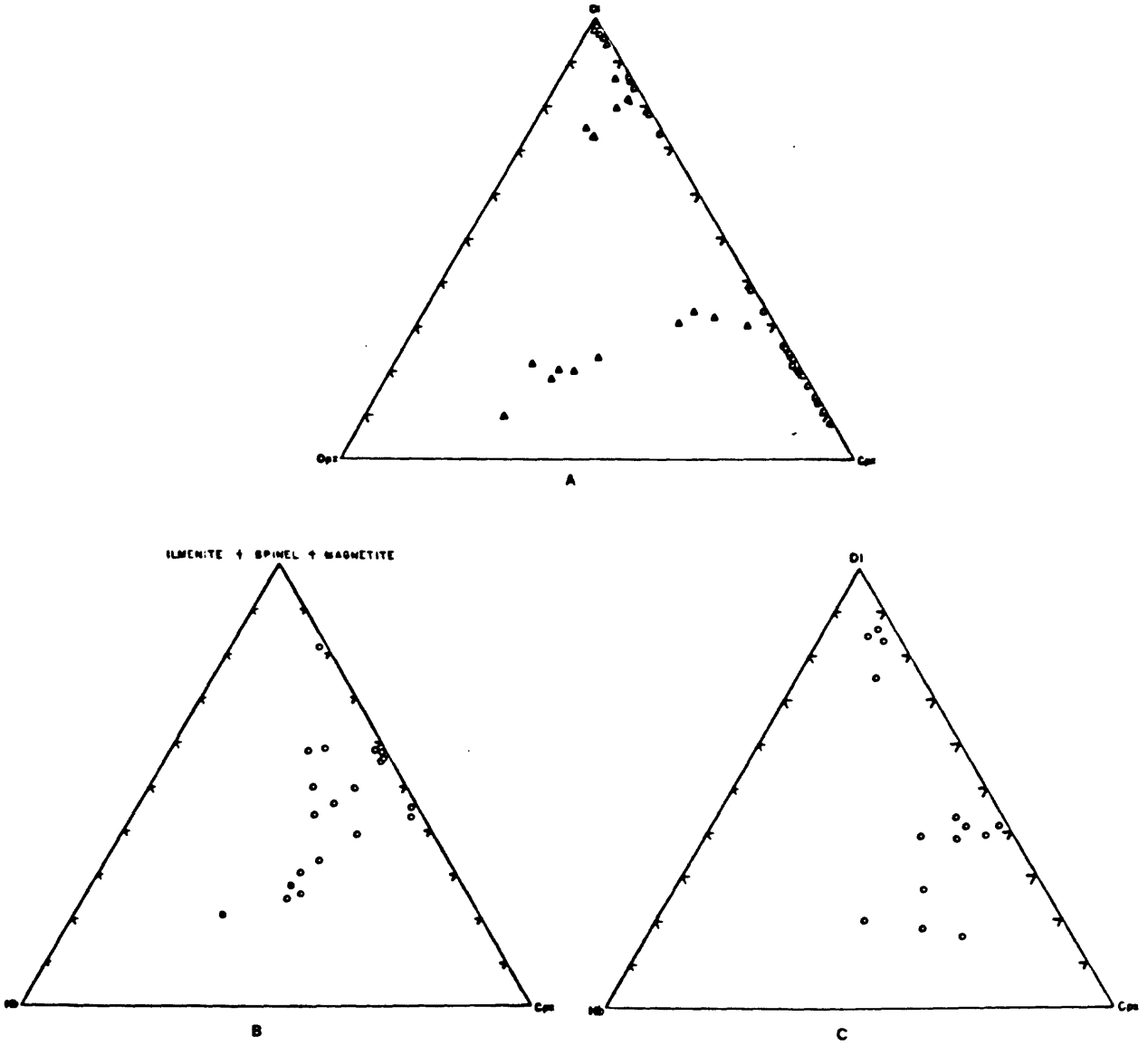

Figure 7. Ternary modal diagrams of ultramafic rocks of wehrlitic (circles) and lherzolitic (triangles) units.

Lherzolitic series

Dunite-lherzolite

Serpentinized dunite and minor lherzolite form the ultramafic rock types in thrust contact with foliated hornblende gabbro in the Tincup Peak ultramafic complex. In the dunites the primary minerals are 91 to 95 percent olivine, 3 to 5 percent clinopyroxene, 0.5 to 1 percent orthopyroxene, and less than 1 percent chromite and magnetite. Minor lherzolite consists of 52 to 45 percent olivine, 44 to 53 percent clinopyroxene, 4 to 10 percent orthopyroxene, and accessory spinel. Discontinuous modal layering can be traced over an entire outcrop (0.5 m).

The thrust contact, placing the ultramafic complex above foliated hornblende gabbro, is exposed continuously for approximately 2.5 km in the western edge of the map area. With the exception of a klippe of brecciated dunite-lherzolite rocks capping Mount Billingslea in the northwestern corner of the mapped area, the thrust contact forms the westernmost extent of ultramafic rocks observed. The shallow-dipping (30-35^{o}) north-northeast trend of the contact has an orientation consistent with that observed in the westward overriding thrust sheets first noted by Irwin (1966) in this region of the Klamath Mountains, and the contact may therefore be a small-scale feature of the dominant stress field evident in his interpretation (see fig. 3).

Along parts of the contact the ultramafic body is altered completely to serpentinite with no relict texture or mineralogy preserved, specifically in the region near Tincup Creek; complete serpentinization is probably due to the easy access for water to hydrate the rocks. More commonly, partially serpentinized dunite is exposed. Preserpentinization textures show a faint foliation and small isoclinal fold hinges in disjointed pyroxene layers. Isoclinal folding is also observed in outcrops at the contact between pyroxene-poor and pyroxene-rich layers in lherzolite (fig. 8). Later crosscutting pyroxenite dikes occur throughout the dunite section (fig. 9). Parts of the unit consist of irregularly mixed dunites with rounded pyroxene clusters (fig. 10). Repeating chromite lenses and alternating pyroxene-rich-pyroxene-poor layers give the unit a distinctive cyclic appearance.

On a microscopic scale, the periodites are medium- to fine-grained rocks composed of equigranular olivine with local variations in grain size due to deformation of large grains that were later partially annealed to a second generation of fine-grained olivine (Nicolas and others, 1971; Wilshire and Pike, 1975; Pike and Schwarzman, 1977). Most of the olivines, however, are altered to serpentine, and rounded polygonal crystal outlines have developed where magnetite was expelled along grain boundaries during the serpentinization process (Haggerty and Baker, 1967; Page, 1967a, b).

The various layers of lherzolite composition have metamorphic porphyroclastic textures with strained 5 to 9 mm clinopyroxene porphyroclasts in a finer grained (<2 mm) matrix of predominantly unstrained recrystallized grains. The strain effects show up chiefly as undulatory extinction; kink bands in pyroxene are present but are much less common than undulatory extinction. Many of the prophyroclasts are composite or glomeroporphyro-

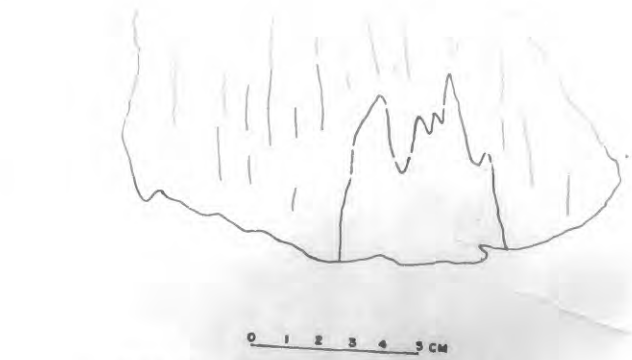

Example of folded layering in ultramafic rocks. Hinge of isoclinal fold shown by olivine-rich layer.

Figure 8.--Hand specimen and sketch of isoclinally folded layer in dunite-lherzolite unit.

Figure 9.--Outcrop of dunite showing crosscutting pyroxenite veins. Near specimen KG182.

Figure 10.--Outcrop of olivine-rich rock with subrounded cluster of pyroxene. Near specimen 78TNC.

clastic, i.e., made up of a collection of irregular-shaped grains. These polymineralic grains are generally rich in clinopyroxene and lesser othopyroxene. Olivine is a minor component. These porphyroclasts are believed to be relict oikocrysts partially destroyed by recrystallization and straining effects. The large grains are commonly alined parallel to the dominant foliation defined by the finer grained minerals in the matrix.

Olivine-diopside heteradcumulate

The olivine-diopside heteradcumulates are located stratigraphically above the dunite-lherzolite unit and constitute the most clearly defined cumulate unit in the Tinup area. These rocks contain approximately 65 percent olivine, 25 percent diopside, 5 to 7 percent orthopyroxene, and 3 percent spinel. One layer of this unit several meters thick can be seen overlying the dunite-lherzolite in the northern portion of the area 0.4 km south of Tincup Creek. In the same area an igneous lamination was noted parallel to the interface between the dunite lherzolite and the heteradcumulate unit. Generally the olivine-diopside heteradcumulates crop out as irregular masses diked extensively by pyroxenites and hornblende gabbro. The best exposures are in the southeastern portion of the map area just south of the plateau area 1 km west of the Gold Basin gravels. The foliation in these exposures is not as well defined as in the exposures near Tincup Peak.

Outcrops of olivine-diopside heteradcumulates are distinctive, displaying on the weathered surface resistant pyroxenes standing uniformly above the olivine grains in an interconnecting system of plateaus and ridges (fig. 11). On fresh surfaces the ridges and plateaus are interstitial anhedral grains of pyroxene (mainly diopside) that flash uniformly, indicating a poikilitic relation to olivine.

Petrographically the unit has a distinctive automorphic-poikilitic texture (fig. 12). Olivine crystals are euhedral 5 to 7 mm grains interlaced by secondary serpentine veins. Diopside forms poikilitic mesostasis textures similar to those found throughout the Ultramafic zone of the Stillwater Complex (Jackson, 1961). Orthopyroxene and spinel are anhedral minor phases in these rocks. Serpentinization is much less extensive in this unit than in surrounding ultramafic rocks. Most of the cumulus olivine grains have interlocking networks of serpentine veins, but completely serpentinized grains are absent. Clinopyroxene shows some retrograding to feathery green hornblende. Except for rare undulating extinction, minor serpentinization, and recrystallization, the olivine-diopside cumulates are devoid of metamorphic effects.

Olivine-orthopyroxene cumulate

This unit consists of 10 to 20 percent olivine, 40 to 55 percent orthopyroxene, 30 percent clinopyroxene, 8 to 10 percent hornblende with accessory magnetite, and 2 percent plagioclase. Exposures of the unit in the area east of the westernmost thrust place it stratigraphically above the olivine-diopside heteradcumulates. Large oikocrysts of clinopyroxene 7 to 15 mm across characterize this unit in the field.

Petrographically, this unit is medium-grained hypidiomorphic granular. The olivines are anhedral irregular phases that are interstitial to the

Figure 11.--Olivine-diopside heteradcumulate. Areas of high relief are interstitial pyroxene. Knife is 8 cm long. Location near specimen 88TNC.

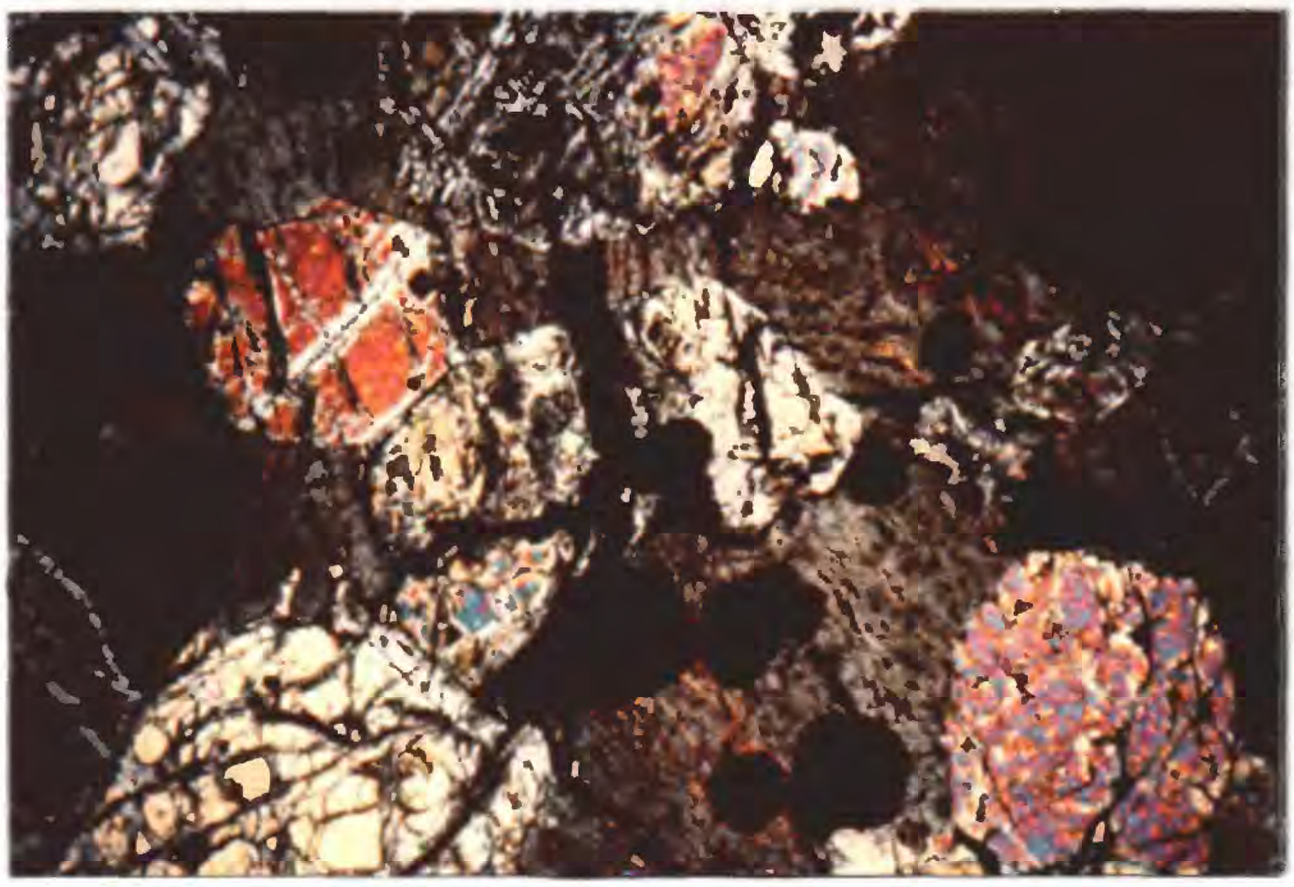

Figure 12.--Photomicrograph showing automorphic-poikilitic texture in olivine-diopside heteradcumulate. Note euhedral form of olivine grains. Specimen 93TNC. Field of view is 3.5 mm across.

euhedral equant orthopyroxene crystals. The plagioclase in these rocks is interstitial anhedral and commonly 3 to 4 mm in grain size (figs. 13, 14). Large oikocrysts are composed mainly of clinopyroxene but some green hornblende oikocrysts were observed.

Wehrlitic series

Wehrlite

Wehrlites in the Tincup Peak complex are coarse-grained rocks, consisting of 40 to 55 percent olivine, 50 percent clinopyroxene, and 5 to 10 percent primary green hornblende. Magnetite occurs in trace amounts. This unit crops out in the eastern part of the ultramafic complex in a thin (several meters thick) discontinous horizon. They are greenish black in color and massive.

Anhedral coarse-grained olivines 1.5 cm across are partially serpentinized. Most of the serpentinization occurs around the edges of the grains; to a lesser degree the cores have veined serpentine formation. Clinopyroxenes (diopside) occur as 0.7 to 1 cm subequant grains with lamellae of orthopyroxene parallel to 100 . Finer grained clinopyroxenes are generally found in the interstices between the larger grains. Green hornblendes are anhedral interstitial. Secondary green hornblende is present as patches in clinopyroxene crystals.

Olivine clinopyroxenite

The olivine clinopyroxenites, the most abundant rock type in the series, are composed of 20 to 25 percent olivine, 75 percent clinopyroxene, 10 to 15 percent green hornblende, and trace amounts of magnetite. These pyroxene-rich rocks crop out as part of numerous lenticular-shaped bodies ranging from 0.6 m to 2 km wide and up to 6.5 km in length. Most of the bodies are northeast trending and appear to be contemporaneous with a series of parallel fractures. One body of olivine clinopyroxenite has been mapped in Gate Saddle.

The texture of the olivine varies from anhedral medium grained to clearly interstitial. Clinopyroxenes are patchy due to alteration by green hornblende; this feature is virtually absent in clinopyroxenes of the lherzolitic series. Orthopyroxene was observed in several sections in trace amounts as partial coronas on olivine grains.

Magnetite clinopyroxenite and hornblende-magnetite clinopyroxenite

The magnetite-bearing clinopyroxenites and the hornblende-magnetite clinopyroxenite are gradational subtypes that are exposed in the easternmost ultramafic body in the mapped area. Both units are medium to coarse grained, well layered, and cyclic.

The magnetite clinopyroxenite is composed of 3 to 5 percent olivine, 55 to 70 percent clinopyroxene, 10 percent hornblende, and 20 to 35 percent magnetite with green spinel. Hornblende-magnetite clinopyroxenite rock consists of 15 to 20 percent clinopyroxene, 60 to 65 percent green hornblende, 10 to 20 percent magnetite with green spinel, and 5 percent plagioclase.

Figure 13.--Photomicrograph of olivine orthopyroxene cumulate. Grain at right is interstitial plagioclase. Orthopyroxene (bronzite) is grain to the left. Specimen KG181. Field of view 2 mm across.

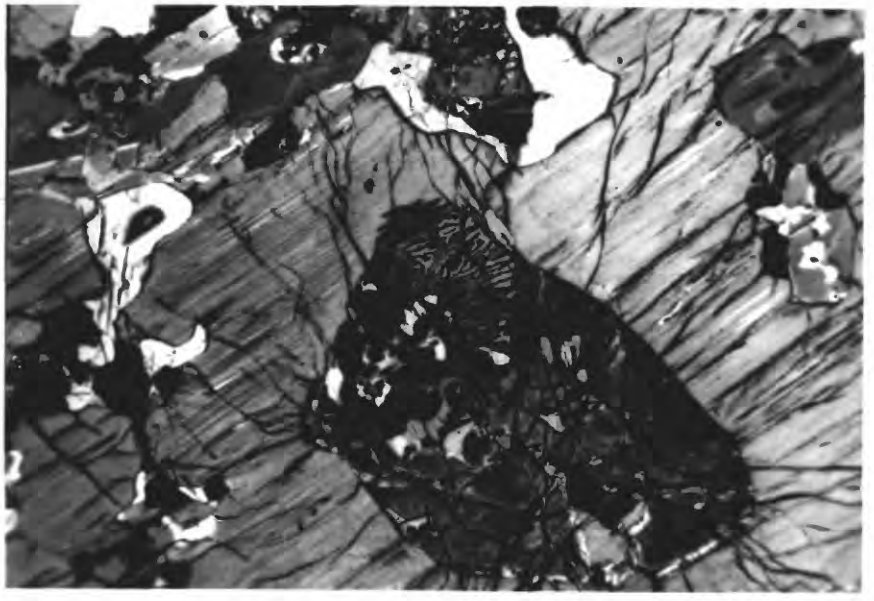

Figure 14.--Photomicrograph of olivine orthopyroxene cumulate. Olivine is inclusion (center) inside clinopyroxene oikocryst. Radial fracture pattern in clinopyroxene developed during serpentinization of olivine grain.

Thin magnetite layers similar to those described at Union Bay (Ruckmick and Noble, 1959) and Duke Island, southeastern Alaska (Irvine, 1974), occur in the southern portion of the map area in the magnetite clinopyroxenite unit. Magnetite in the hornblende-magnetite clinopyroxenites is disseminated, fine to coarse grained, anhedral, interstitial to diopside, and generally evenly distributed throughout the rocks. Although this unit is layered and has sequences of graded beds (fig. 15), no monomineralic magnetite layers were observed.

Gabbroic rocks

Lherzolitic series

The two-pyroxene cumulus gabbroic rocks of the lherzolitic series are medium grained and equigranular, and they consist of 50 to 65 percent plagioclase, 20 to 25 percent clinopyroxene, 10 to 20 percent orthopyroxene, and 3 to 5 percent magnetite, with rare olivine and hornblende. This gabbroic unit is predominant in the extreme eastern portion of the Tincup Peak area and its outcrop pattern suggests that it is continuous beneath the Gold Basin gravels. It crops out in other portions of the area as massive layers alternating on a large scale with the poikilitic olivine orthopyroxene cumulate. The best exposures of the two-pyroxene gabbro occur on the ridge just above the confluence of the Tincup Creek tributaries where the gabbro is thrust over a clinopyroxenite body (fig. 16). The poikilitic character of the gabbro is strongest in the western portion of the area, becoming a rare feature in the southeastern exposures around Gold Basin. Modal layering in the outcrop occurs on a scale of 1 to 9 cm and is caused by variations in the ratio of pyroxene to plagioclase.

Seen in thin section, plagioclase crystals typically range from 0.7 to 2 mm subhedral grains with albite and pericline twinning. Clinopyroxene, the second most abundant mineral in the gabbro, occurs in 2.3- to 3-mm size crystals which enclose numerous crystal inclusions typically about 1 mm in length (fig. 17). The inclusions are composed mainly of euhedral plagioclase crystals. Orthopyroxene forms small equant crystals approximately 2 mm in size that are highly pleochroic, pink to pale green. Hornblende, epidote, and sericite are common secondary minerals.

Wehrlitic series; hornblende gabbro

Gabbroic rocks assigned to the wehrlitic series typically consist of 55 to 71 percent plagioclase, 25 to 40 percent green hornblende, and 2 to 5 percent magnetite. Clinopyroxene is found in trace amounts in the cores of the hornblende crystals. The high hornblende content, absence of orthopyroxene, and near absence of clinopyroxene, distinguish these rocks from the gabbros of the lherzolitic series. The hornblende gabbro crops out in greatest abundance in the southwestern portion of the mapped area and forms the sharp crests of Tincup Peak. With the exception of the local massive Tincup Peak outcrops, most occurrences of the gabbroic rock are dikelike in nature. The unit forms intrusive breccias in the Gate Saddle area and in an 0.6 km stretch along the canyon walls of Tincup Creek.

Figure 15.--Photograph of crude layering in hornblende magnetite clinopyroxenite. Sample 67TNC.

Figure 16.--Outcrop of banded two-pyroxene gabbro. Knife at left is 8 cm long. Location near specimen 107TNC.

Figure 17.--Photomicrograph of two pyroxene gabbro showing clinopyroxene crystal (in extinction). Note numerous small inclusions of tabular plagioclase, rare orthopyroxene. Length of view is 4 mm.

The hornblende gabbro is perhaps the most distinctive unit in the field, consisting of euhedral coarse-grained black hornblende crystals (3-11 cm X 0.5-1 cm) in a matrix of grayish-white to milky-white feldspar. The hornblende shows three distinct habits: oriented prisms, comb structure, and random pegmatitic texture. Oriented prisms of hornblende are typically 1.5 cm long with their long axes parallel. Comb structures are characterized by hornblendes oriented perpendicular to dike walls (or possibly crude layering; fig. 18). Commonly the dikes are separated by irregular lenses of fine-grained hornblendite. Similar intradike material has been described in the southern part of Duke Island and considered "country rock septa" by Irvine (1974, p. 54). Random pegmatite texture consists of coarse-grained subhedral to anhedral hornblende randomly oriented in a milky-white matrix of altered feldspar.

A local troctolitic variety of the hornblende gabbro crops out south of Tincup Peak. This rock consists of 60 to 70 percent coarse anhedral feldspar, 25 to 35 percent anhedral olivine, 3 to 5 percent green hornblende, and trace amounts of pyroxene, anthophyllite, magnetite, and green spinel. Exposures of the troctolite occur in zones that contain large xenoliths of ultramafic rock (fig. 19).

Jorgenson (1970, 1971), in his study of the petrology and origin of the Illinois River Gabbro, also described troctolites similar to these.

Microscopically, the hornblende prisms in the hornblende gabbro have euhedral to subhedral form in both the oriented prism and the comb structure variety. The plagioclase occurs as 1.5- to 3-mm crystals clustered between large hornblendes. Magnetite typically occurs as interstitial crystals. In the pegmatite variety the hornblende is anhedral and coarse grained. Plagioclase occurs as fine crystals with irregular borders.

Foliated hornblende gabbro

A foliated, medium-grained, light-gray rock underlies the ultramafic-gabbroic terrane. The rock consists of 40 percent subhedral hornblende, 58 percent plagioclase, and trace amounts of magnetite. Some of the plagioclase crystals are partially altered to epidote. Major exposures of the foliated hornblende gabbro occur in the westernmost region of the mapped area and form a tectonic contact with overlying ultramafic rocks. The foliation in the gabbro is parallel to the contact between the two rocks.

Caught up in this contact zone are irregular bodies of extremely fine grained banded gneiss consisting of quartz+plagioclase+orthopyroxene with rare brown biotite. The gneiss is welded to the foliated hornblende gabbro. The origin of this rock type is presently unknown, but this unit mostly represents fragments of siliceous dikes caught up in the thrust zone.

Granites

A medium-grained granite is exposed in the southwestern portion of the mapped area and in exposures in Tincup Creek near its confluence with Lucky Creek. The granite is an altered muscovite-bearing granite and is massive in texture.

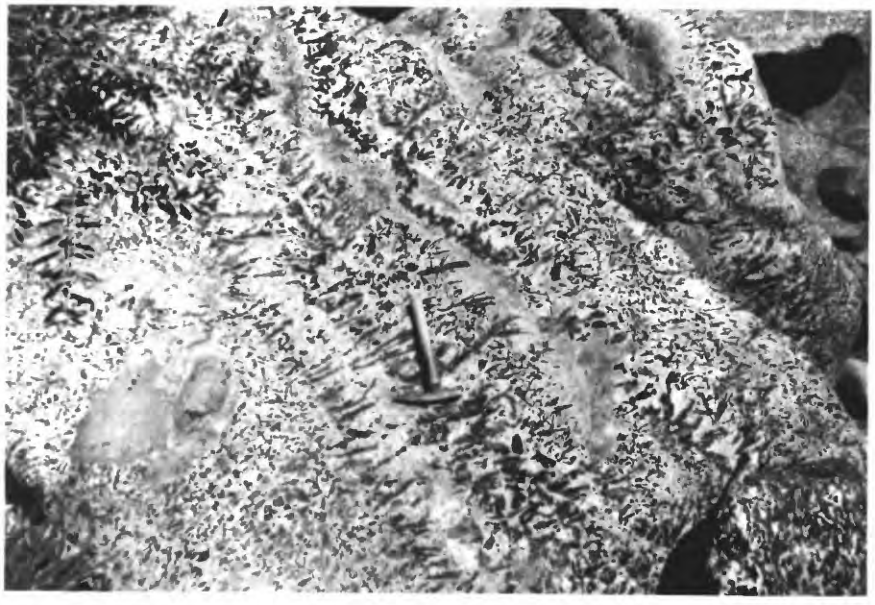

Figure 18.--Outcrop of hornblende gabbro showing comb-textured variety of hornblende near specimen 45TNC.

Figure 19.--Olivine-bearing hornblende gabbro with xenoliths of recrystallized ultramafic rock near specimen 110TNC.

Mafic dikes

Late-stage dikes ranging from slightly recrystallized diabase to granite crosscut earlier rock bodies located in the ultramafic-gabbroic block and in the foliated hornblende gabbro. The dikes commonly exhibit plastic flow foliation and deformation. Both ground survey and aerial photograph scanning reveal that most of the dikes lie along major fault structures.

Primary igneous features

lherzolitic series

Compositional layering and coarse poikilitic crystals occur throughout the lherzolitic series. Compositional layering occurs in the dunite lherzolitic unit as cumulus chromite-rich layers 0.3 to 0.7 cm thick, interlayered with olivine-rich zones approximately 1 m thick. This sequence is repeated at least three times in the western portion of the map area.

Poikilitic texture is common in the olivine-clinopyroxene heteradcumulate, the olivine orthopyroxene cumulates, and the two-pyroxene gabbro. Oikocrysts of pyroxene are roughly spherical in shape and range in size from 0.8 mm to 12 cm in diameter.

Wehrlitic series

Graded, modal, and compositional layering are characteristic of the wehrlitic series. Graded rhythmic layering is shown in figure 15. Textures show that tops face to the east. Complete cycles are repeated as many as seven times and are approximately 1.3 m thick. Modal and compositional layering occur throughout the magnetite clinopyroxenite and hornblende-magnetite clinopyroxenite members. Magnetite layers vary from approximately 0.3 to 1 cm in thickness.

The comagmatic association of the ultramafic and gabbroic rocks in the wehrlitic series is shown by similarity in orientation of layers and textural-mineralogical features such as coarse grain size (fig. 20), primary hornblende, and virtual absence of orthopyroxene.

Comparisons

The two rock series at Tincup Peak display differing large-scale trends in the spatial distribution of what is believed to be their crystallization history. If the late, disruptive intrusives (mafic dikes, hornblende gabbro) are subtracted, a reconstruction of the two series shows that: (1) the lherzolitic series is younger toward the east; and (2) the wehrlitic series ultramafic rocks are younger toward the center.

Dunite-lherzolite in the western edge of the lherzolitic unit grade progresssively into layered two-pyroxene gabbro. Petrographic features show the series to be generated by the sequential crystallization of olivine$\pm$chromite, clinopyroxene, orthopyroxene, magnetite$\pm$hornblende, hornblende, and plagioclase (fig. 21).

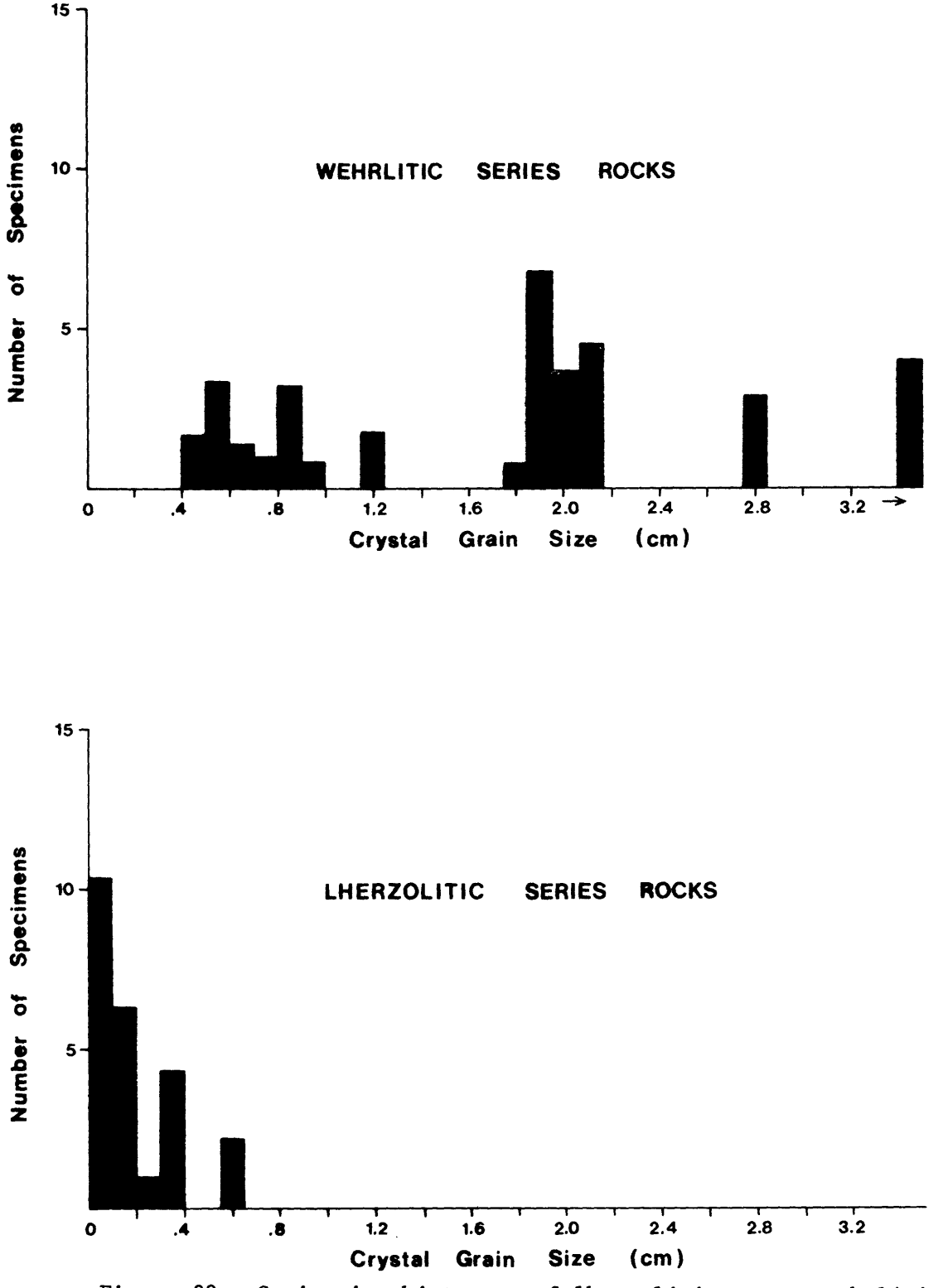

Figure 20.--Grain size histogram of lherzolitic versus wehrlitic rocks. The grains in a hand specimen were measured and then averaged for each count. Note that there is only minor overlap (0.4-0.8 cm) between the two series.

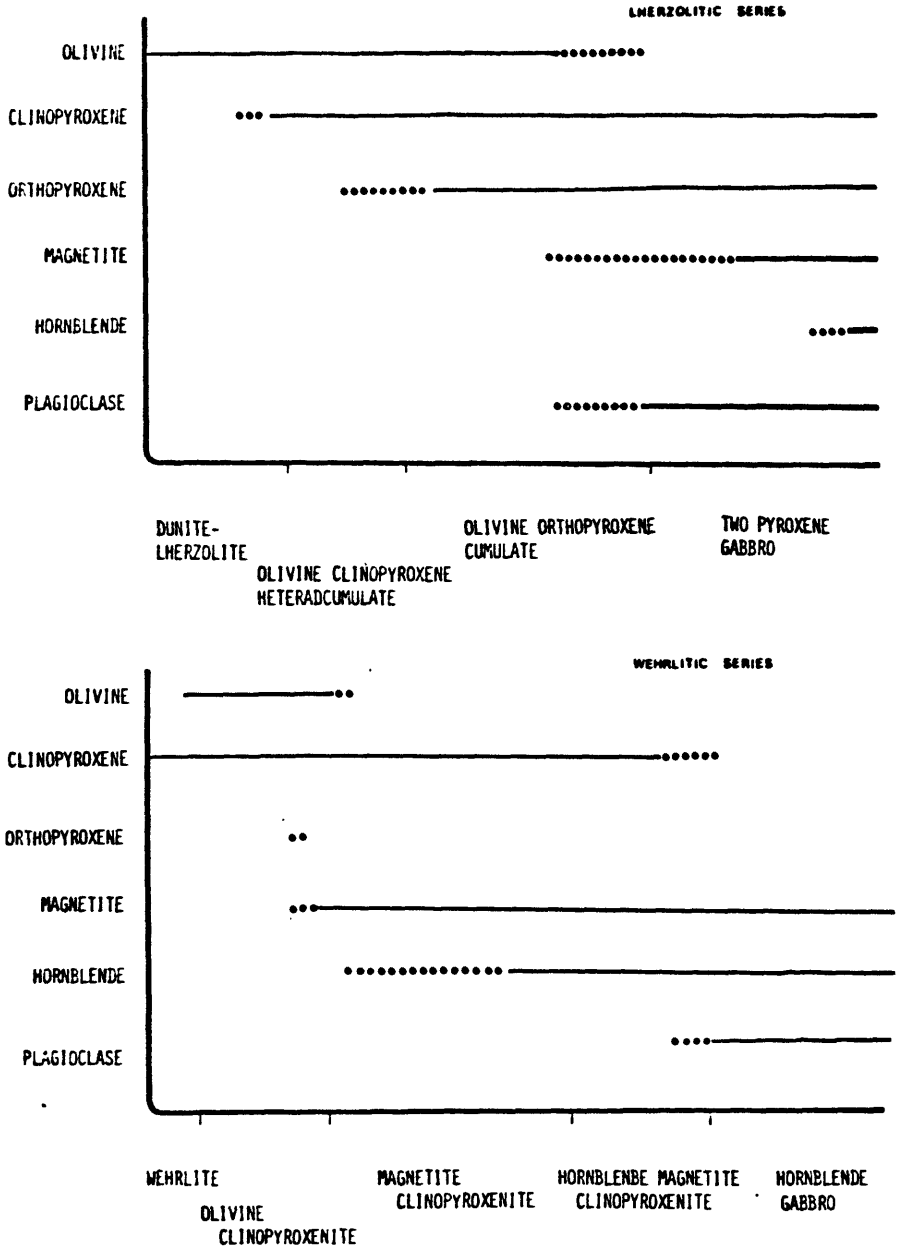

Figure 21.--Mineral crystallization models for Tincup Peak rocks. The order in which the minerals fractionated is from top to bottom or left to right.

Noncumulus wehrlite and olivine clinopyroxenite along the east and western borders of the wehrlitic series grade into hornblende magnetite clinopyroxenite with trace amounts of plagioclase. Petrographic data support the sequential crystallization of the minerals olivine+clinopyroxene, magnetite±spinel, hornblende, and plagioclase.

STRUCTURAL GEOLOGY

Tectonic setting

The Klamath geologic province occurs along the western edge of the Cordilleran mobile belt and spans equal areas in southwestern Oregon and northern California. The Klamath structural pattern is a large westwardly convex arc of lithologic and formational belts often referred to as the Mendocino Orocline (Davis, 1963, 1964, 1968, 1969). Diller (1902), Taliaferro (1942), Irwin (1964), Kays (1970), and others noted a younger westward trend among the arcuate belts of the Klamath rocks. Dott (1971) suggests that near the southwestern Oregon coast the major thrusting took place in mid-Cretaceous and possibly early Tertiary, culminating a Jurassic and Early Cretaceous period of intense structural deformation. Northwest-trending vertical faults, possibly related to the San Andreas system, were later superimposed on the older structural features in the Late Cenozoic (fig. 22).

In the Tincup Peak area there are three basic sets of structural features. These features are classified here as S_1, layering of igneous bodies; S_2, prominent east- to northeast-dipping thrust faults with accompanying minor folds; and S_3, a later set of northwest-trending steep to moderately dipping normal faults.

Layering, S_1

Layering is present throughout the olivine clinopyroxenite and hornblende-magnetite clinopyroxenite rock of the wehrlitic series. It occurs sporadically in the olivine-clinopyroxene heteradcumulates and two-pyroxene gabbro of the lherzolitic series. Figure 21 is an equal area projection of poles to layering for various sections of the mapped area. Sections I and II in eastern exposures of the two-pyroxene gabbro and in the clinopyroxenite-rich unit, respectively, plot as clusters (figs. 23a, b). The layering in section III, near the western thrust, is a crudely defined shallow-dipping synclinal structure (fig. 23c). The orientation of the pole to the great circle of poles to layering is S. 41° W. at 9°.

Thrust faults, S_2

Thrust faults form the primary contact in the western portion of the area between foliated hornblende gabbro and the ultramafic terrane. A second parallel thrust, partially obscured, forms the contact between the clinopyroxenite unit and a massive block of banded two-pyroxene gabbro in the east.

These thrusts are secondary imbricate structures related to the regional Jurassic boundary fault (see fig. 3). The extent of the thrusting is uncertain but a klippe of peridotite to the west (1.6 km) forms the peak of

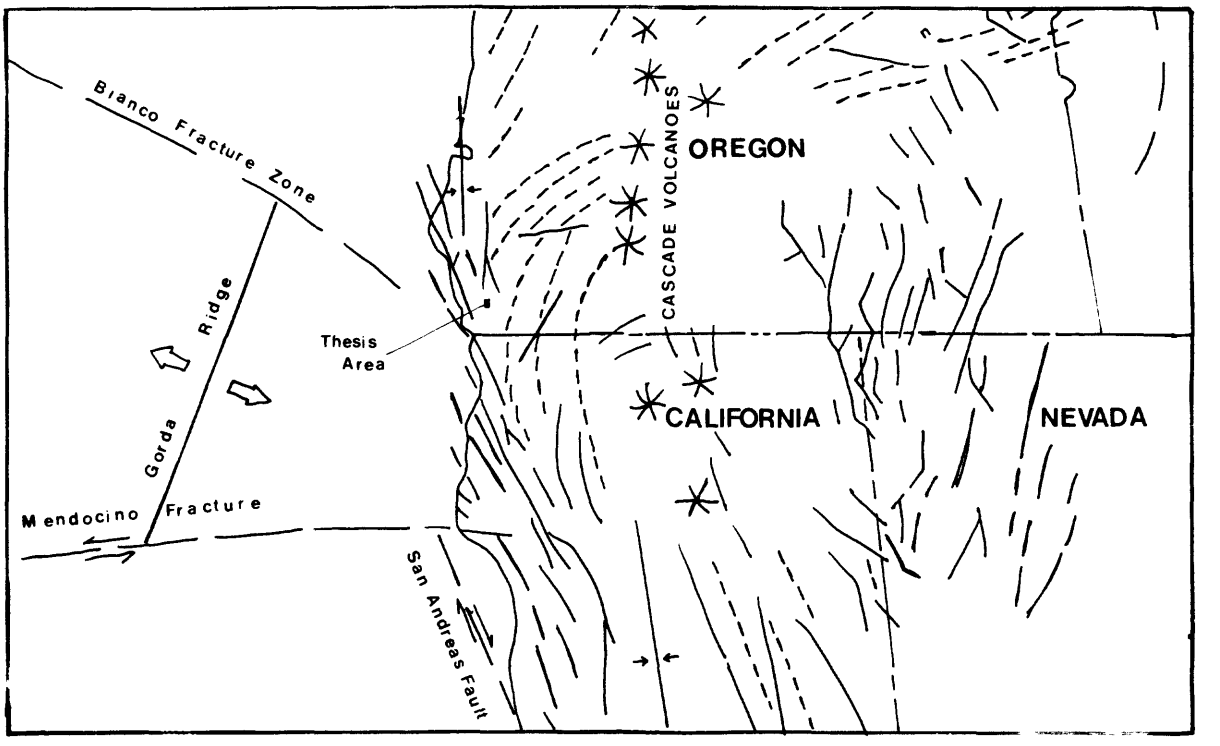

Figure 22.--Tectonic setting of southwestern Oregon and adjacent oceanic crust. Note Cenozoic arcuate structural pattern (dashed lines) and the superiposed, late Cenozoic cascade volcanic arc (stars) and faulting (heavy lines). Modified from Dott (1971).

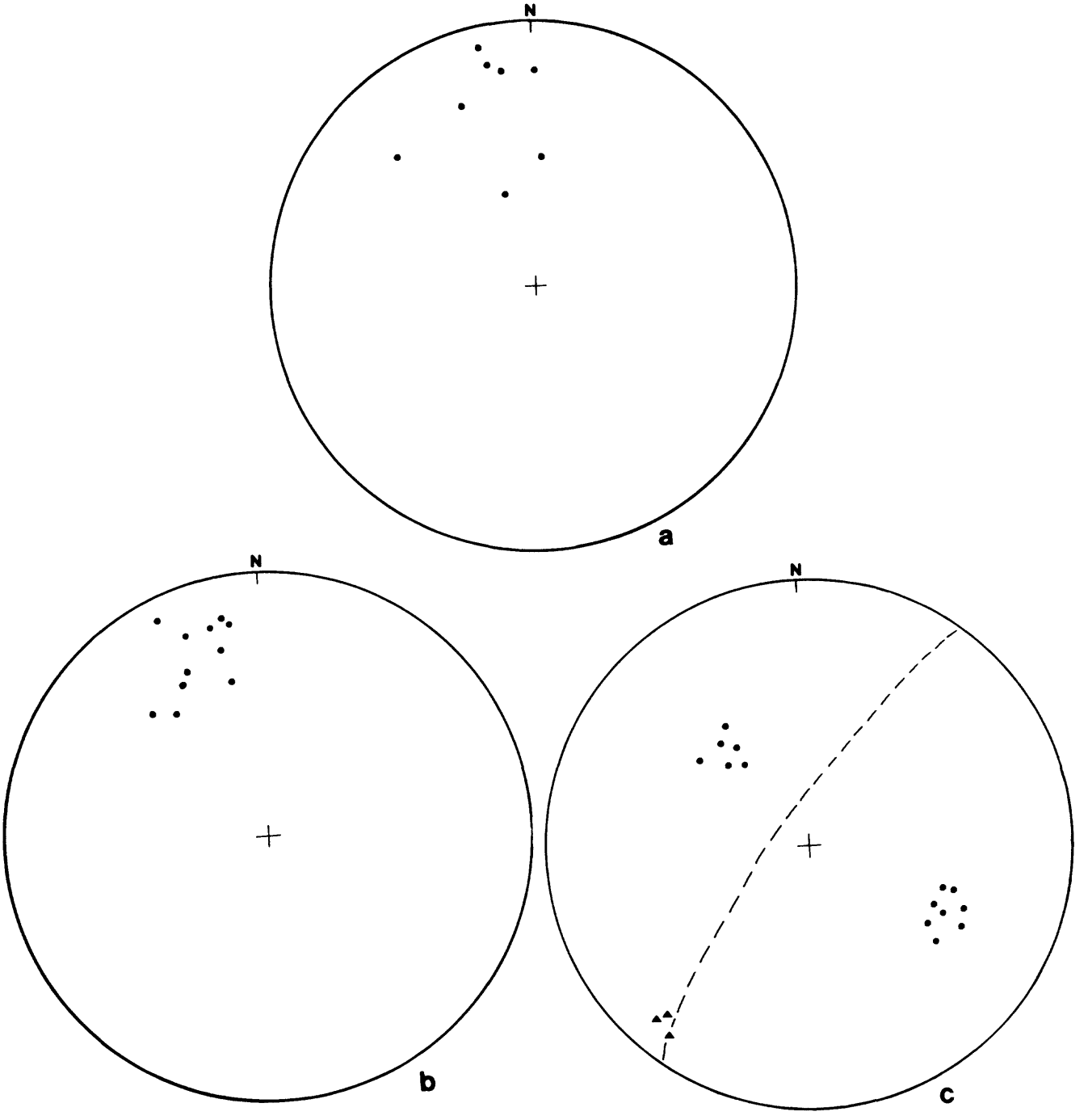

Figure 23.--Lower hemisphere equal area projections of foliations in gabbroic and ultramafic rocks. Closed circles = poles to foliation; closed triangles = minor fold axes. A, Poles to foliation in two pyroxene gabbro (defined by phase layering); B, Poles to foliation in clinopyroxenite (wehrlitic series); C, Poles to foliation in lherzolitic rocks near westernmost thrust.

Mount Billingslea. The klippe is lithogically similar to the Tincup Peak dunite-lherzolitic rock and is crosscut by mafic intrusives identical to those found in the main ultramafic complex.

In the southern half of the area, thrusting places the ultramafic-mafic complex over foliated hornblende gabbro and granitic rocks. This fault zone is characterized by large shear zones with felsic sulfide-bearing dikes (see fig. 24).

Later faults, S_3

Steeply dipping, northwest-trending faults offset the major thrust contacts. The faults are sharply discordant to the layering and contacts of the major rock units. The crosscutting faults are commonly accompanied by mafic to felsic dikes that are commonly mylonitized. Small dikes of hornblende gabbro exhibit cataclastic textures within these structures.

Minor northeast-trending shears and slickensides occur along the contacts of the lithologically different rock units.

MINERALOGY

Chemical analyses of the primary mineral phases of the igneous complex at Tincup Peak were made at the University of Massachusetts, Amherst, with the ETEC Autoprobe electron microprobe. Natural and synthetic standards were used, data being corrected for absorption and fluorescence using a program modified from Bence and Albee (see Bence and Albee, 1968; Albee and Ray, 1970). Operating conditions were 15 kv excitation potential and 0.03 microampere aperture current.

Olivine

Representative composition ranges of typical olivines are given in table 1 and figure 25. The compositions of olivine in the two series overlap; lherzolitic and wehrlitic rocks show a range in Fo content from Fo_{74} to Fo_{82}. The Fo values for the analyzed olivines are illustrated in figure 16 where these ratios are compared with those in other ultramafic complexes. The olivines of the Tincup Peak complex are more iron rich than those of typical Alpine type peridotites (tectonites) whose restricted Fo compositions lie between Fo_{94} and Fo_{88} (Green, 1964; Challis, 1965, 1966; Jackson and Thayer, 1972; Dick, 1976). Olivines from the zoned ultramafic complexes of Alaska and the Greenhills ultramafic complex, New Zealand, most nearly approximate the composition of the Tincup Peak olivines.

Orthopyroxene

Orthopyroxene analyses are listed in table 2 and summarized in figure 26. The amount of Al in orthopyroxene is slightly lower in the lherzolitic series, averaging approximately 1.18 weight percent as compared with 1.94 weight percent for wehrlitic series rocks. Generally for the lherzolitic series, the orthopyroxenes are bronzite in the ultramafic rocks and hypersthene in gabbroic rocks.

Figure 24.--Shear zone in northwest-trending thrust fault. Photograph shows felsic dike with Boudin shape. Knife is 8 cm long. Near specimen 17.

Table 1. Electron probe analyses of olivine

	Lherzolitic series			Wehrlitic series		
Sample	123BTNC	121TNC	6TNC	47TNC	69TNC	45TNC
SiO_2 ------	40.82	33.9	36.82	35.75	34.71	34.89
TiO_2 ------	0.01	-	0.06	0.01	0.04	0.01
Al_2O_3 -----	-	0.06	0.05	-	0.02	0.01
Cr_2O_3 -----	-	0.01	0.06	0.01	0.05	-
FeO* ------	15.19	23.31	22.07	17.26	22.52	21.19
MnO -------	2.08	2.34	0.47	1.7	2.28	2.77
MgO -------	43.7	40.82	39.99	45.43	40.38	41.33
CaO -------	0.01	0.01	0.04	0.01	0.0	-
Na_2O ------	-	0.08	-	-	0.05	-
Total -----	101.81	100.53	99.56	100.17	100.02	100.19
	Cations per four oxygens					
Si --------	1.012	0.873	0.957	0.922	0.922	0.921
Ti --------	-	0.002	0.001	-	0.001	-
Al --------	-	-	0.001	-	-	-
Fe --------	0.315	0.502	0.478	0.372	0.501	0.468
Mn --------	0.04	0.051	0.010	0.037	0.051	0.060
Mg --------	1.616	1.567	1.547	1.747	1.6	1.627
Ca --------	-	-	0.001	-	-	-
Na --------	-	0.004	-	-	0.002	-
cations -	2.983	2.999	2.995	3.078	3.077	3.076
Fo --------	82.0	73.9	76.0	81.0	74.3	75.4

Sample$^+$ = see appendix for listing of sample rock type.

FeO$^+$ - Total Fe as FeO.

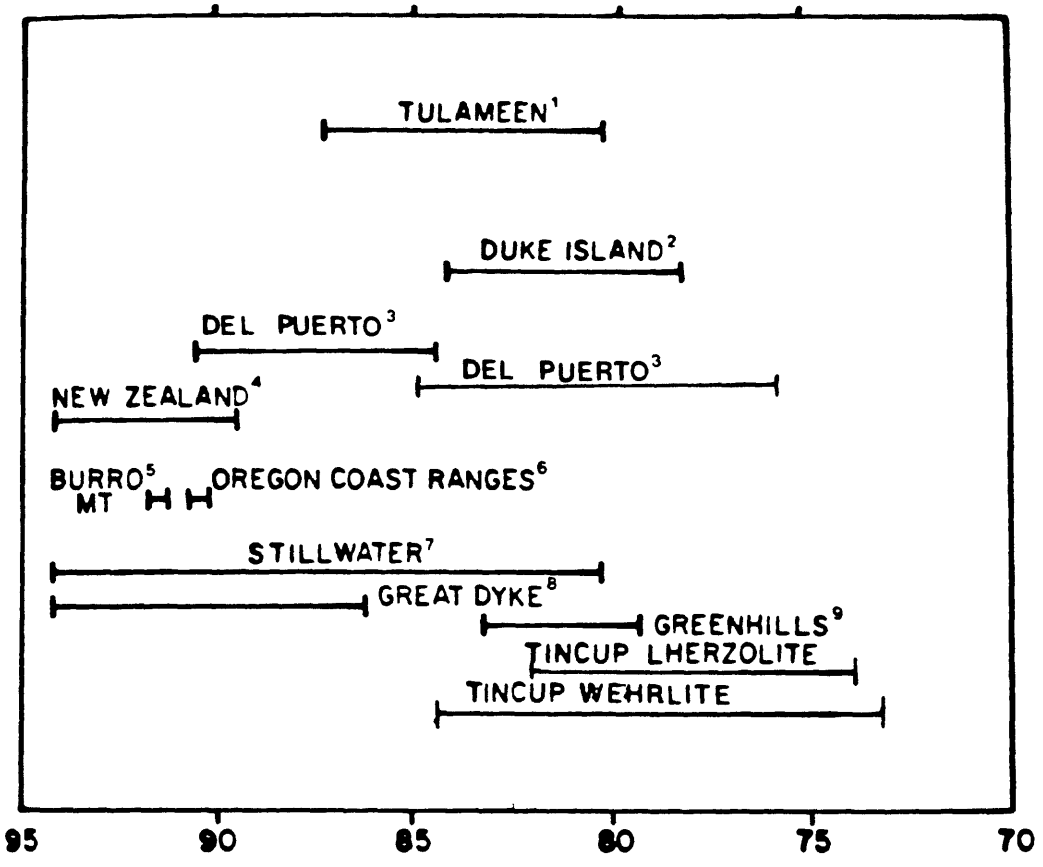

Figure 25. Diagram comparing olivine compositions in several varieties of ultramafic occurrences with the ultramafic complex at Tincup Peak.

1. From Findlay (1969)
2. From Irvine (1959, 1963, 1967)
3. From Himmelberg and Coleman (1968);Evarts (1977)
4. From Challis (1965)
5. From Loney and others (1971); Page (1967)
6. From Bailey and Blake (1974); Himmelberg and Coleman (1968)
7. From Hess (1960)
8. From Worst (1960)
9. From Mossman (1973)

Table 2. Electron probe analyses of orthopyroxene

	Lherzolitic series		Wehrlitic series		
Sample	121TNC	92TNC	KG187	69TNC	45TNC
SiO	52.95	47.52	50.40	46.71	50.76
TiO_2	0.01	0.13	0.05	0.03	-
Al_2O_3	1.24	1.12	1.50	2.69	1.62
Cr_2O_3	0.02	-	0.03	0.01	0.01
FeO*	16.04	22.77	15.7	16.16	13.14
MnO	3.18	3.63	2.9	2.45	2.71
MgO	26.66	23.14	26.89	30.89	30.8
CaO	0.14	1.53	0.6	0.64	0.25
Na_2O	0.02	-	-	0.01	-
Total	100.52	99.84	98.07	99.6	99.29
	Cations per six oxygens				
Si	1.913	1.773	1.857	1.665	1.811
Al	0.053	0.049	0.065	0.113	0.068
Fe^{3+}	0.034	0.178	0.078	0.222	0.121
	2.000	2.000	2.000	2.000	2.000
Ti	-	0.004	0.001	0.001	-
Al	-	-	-	-	-
Cr	0.001	-	0.001	-	-
Fe^{3+}	0.088	0.219	0.138	0.260	0.189
Fe^{2+}	0.362	0.314	0.268	-	0.082
Mn	0.097	0.115	0.091	0.074	0.052
Mg	1.435	1.287	1.477	1.641	1.637
Ca	0.015	0.068	0.024	0.024	0.010
Na	0.001	-	-	0.001	-
	1.999	2.000	2.000	2.001	2.000
Mg*	0.712	0.609	0.720	0.747	0.775
Wo	0.008	0.037	0.014	0.014	0.006
En	0.792	0.774	0.835	0.986	0.947
Fs	0.002	0.189	0.151	-	0.047

FeO* = Total Fe as FeO

Mg* = $Mg/Mg + Fe_{total} + Mn$

Clinopyroxene

Clinopyroxene analyses are shown in table 3 and figure 26. Oxide totals range from 99.13 to 100.48 weight percent. The clinopyroxenes show a limited trend toward Fe enrichment. The Al_2O_3 content ranges from 1.59 to 2.48 weight percent in clinopyroxenes of lherzolitic rocks and from 1.84 to 5.1 weight percent in wehrlitic rocks. Figure 27 shows the variations of several oxides plotted against atomic Mg.

Several clinopyroxene analyses yield a ratio, Ca:(Ca+Mg+Fe), less than 0.5. This ratio may infer low silica activity and reflects the combination of abundant Ca-Tschermaw's molecule ($CaAl_2SiO_6$) with low enstatite ($Mg5:O_3$) and ferrosilite ($FeSiO_3$) (Irvine, 1973, p. 488).

Plagioclase

Analyses of plagioclase from Tincup Peak are presented in table 4 and figure 28. Small amounts of plagioclase are present in both wehrlitic and lherzolitic ultramafic rocks. Plagioclase compositions in gabbroic rocks of the wehrlitic series range from $An_{95.4}$ to $An_{96.2}$. The An values for the lherzolitic rocks range from $An_{96.1}$ to $An_{79.5}$. One plagioclase analysis from the foliated metagabbro, sample 75TNC77, has a composition of An_{92}. Minor Fe is present in all plagioclase but shows no good correlation with An content.

Amphibole

Electron microprobe analyses and cation totals of hornblende are shown with total Fe as FeO in table 5. Hornblende mineral formulae were calculated from the microprobe analyses using a Fe^{3+} correction procedure that normalizes the M 1, 2, 3, and tetrahedral cations to a sum of 13.0. A stoichiometry of 23 oxygens was assumed.

Spinel

Spinel analyses for Tincup Peak samples are given in tables 6 and 7. Chromitic spinel, table 6, was found only in the lherzolitic series. Discrete primary spinels are Fe-rich ferrochromites; Fe:Mg ratios are greater than 2:1.

Hercynitic spinels, table 7, are found in both rock series. Representative samples show that Mg:Fe ratios are higher in the wehrlitic series than in the lherzolitic series. Chromium enters the spinel structure to a greater extent in the lherzolitic series.

Magnetites and ilmenites

Representative electron microprobe analyses and cation totals are given in table 8. Magnetite and ilmenite compositions are plotted in terms of Fe_3O_4-Fe_2O_3-TiO_2 in figure 29; they are consistent with low-temperature subsolidus equilibration.

Table 3. Electron probe analyses of clinopyroxene

	LHERZOLITIC SERIES			WEHRLITIC SERIES		
Sample	123TNC	93TNC	121TNC	92TNC	7TNC	80TNC
SiO_2 -----	53.16	52.15	50.12	49.34	50.92	51.97
TiO_2 -----	-	0.29	0.12	0.23	0.26	0.12
Al_2O_3 ----	1.59	1.68	2.48	1.84	5.1	3.25
Cr_2O_3 ----	0.11	0.01	0.03	-	0.08	0.23
FeO* -----	3.25	4.18	7.23	9.01	5.53	4.64
MnO ------	0.89	0.88	1.5	1.67	0.16	0.52
CaO ------	24.24	23.47	23.44	23.21	23.02	23.18
NaO_2 -----	-	0.05	-	0.37	0.22	0.1
Total ----	99.13	99.42	100.35	100.48	100.06	100.3
	CATIONS PER FOUR CATIONS					
Si -------	1.964	1.918	1.846	1.822	1.828	1.895
Al -------	0.036	0.073	0.108	0.080	0.172	0.105
Fe^{3+} -----	-	0.009	0.046	0.098	-	-
	2.000	2.000	2.000	2.000	2.000	2.000
Ti -------	-	0.008	0.003	0.006	0.007	0.003
Al -------	0.033	-	-	0.002	0.048	0.035
Cr -------	0.003	-	0.001	-	0.002	0.007
Fe^{3+} -----	0.10	0.069	0.146	0.18	0.122	0.064
Fe^{2+} -----	-	0.051	0.030	-	0.047	0.077
Mn -------	0.028	0.027	0.047	0.052	0.005	0.016
Mg -------	0.875	0.916	0.847	0.815	0.851	0.885
Ca -------	0.960	0.925	0.925	0.919	0.902	0.906
Na -------	-	0.004	-	0.026	0.016	0.007
	1.999	2.000	1.999	2.000	2.000	2.000
Mg* ------	0.873	0.826	0.730	0.712	0.838	0.849
Wo -------	0.496	0.460	0.464	0.456	0.443	0.469
En -------	0.452	0.456	0.425	0.405	0.469	0.458
Fs -------	0.052	0.083	0.111	0.138	0.088	0.073
Ca + Na/2	0.480	0.465	0.463	0.476	0.459	0.457

FeO* = Total Fe as FeO

Mg* = $Mg/Mg + Fe_{total} + Mn$

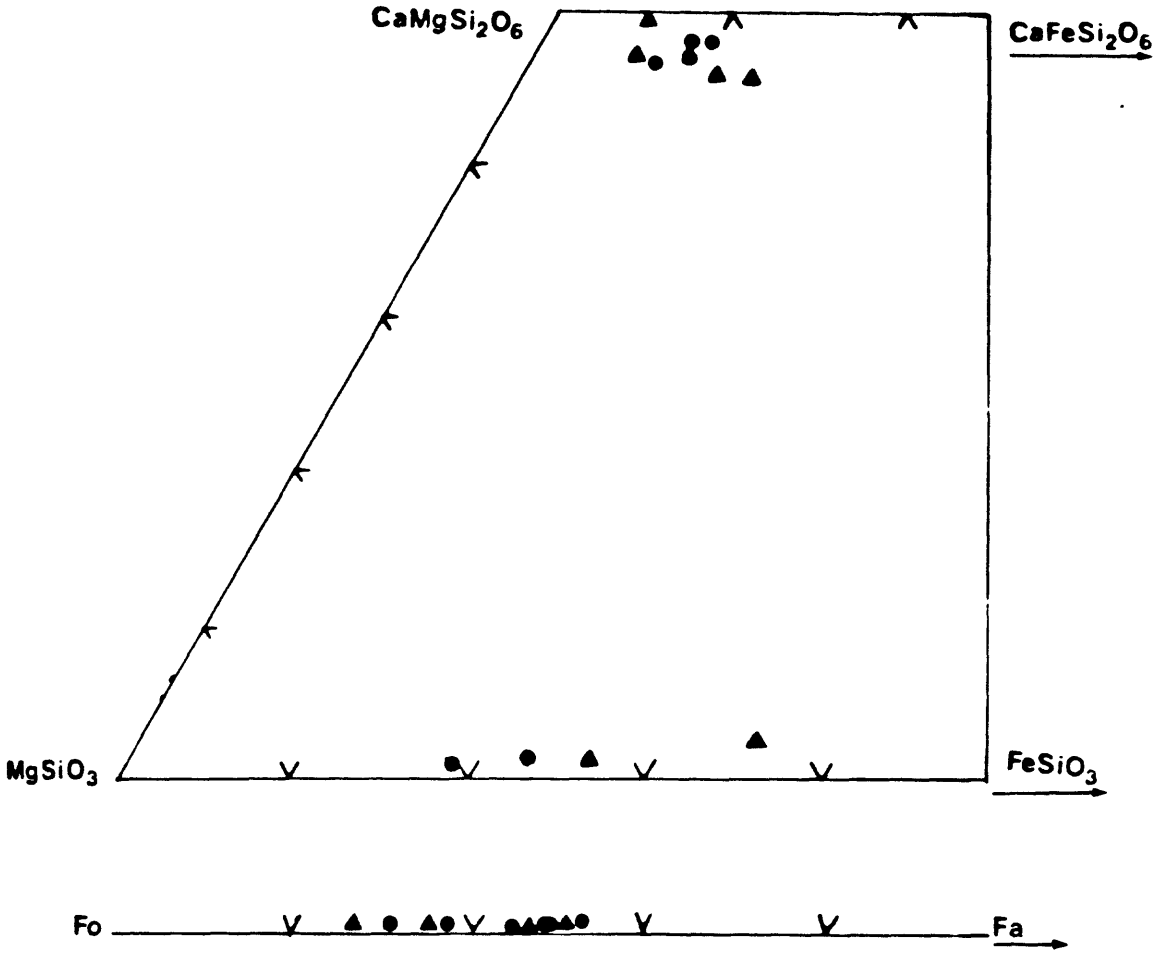

Figure 26.--The pyroxene gradulateral with microprobe compositions of Tincup Peak pyroxenes. Closed circles = wehrlitic series pyroxenes; closed triangles = lherzolitic series pyroxenes. Olivine compositions are plotted at bottom.

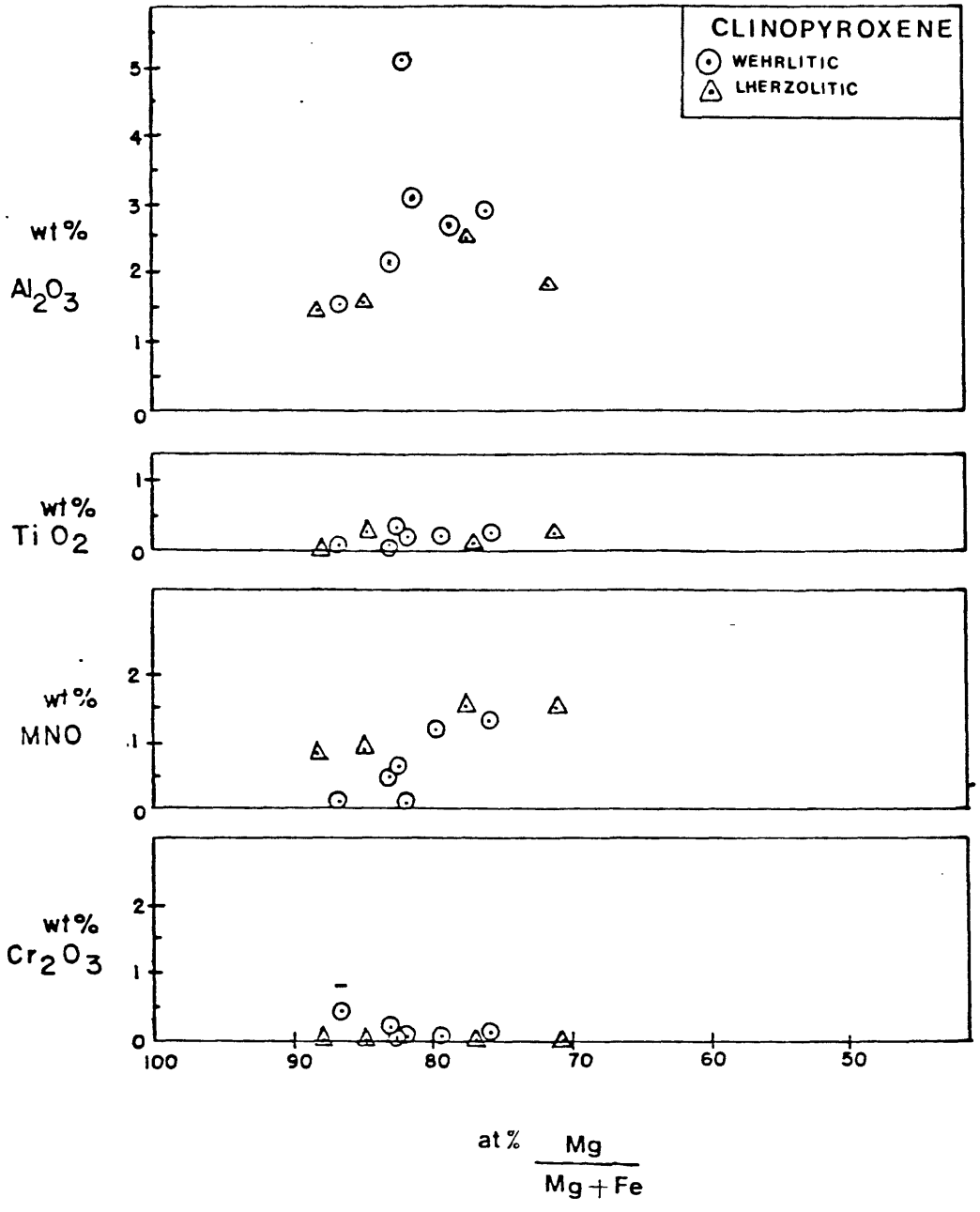

Figure 27.--Chemistry of clinopyroxenes plotted in terms of minor oxides versus Mg ratio.

Table 4. Electron probe analyses of plagioclase

	Lherzolitic series			Wehrlitic series		Foliated hornblende gabbro
Sample	92TNC	97TNC	KG181	44TNC	73TNC	75TNC
SiO_2 --	46.86	42.85	45.26	43.51	41.8	45.61
TiO_2 --	-	0.05	-	-	-	-
Al_2O_3 -	33.3	37.28	35.71	35.42	36.53	32.86
FeO ---	0.23	0.11	0.31	0.14	0.45	0.11
CaO ---	17.1	19.38	18.11	19.67	20.34	19.64
NaO ---	2.41	0.55	0.39	0.51	0.75	0.93
K_2O ---	0.05	0.02	0.02	-	0.01	0.02
	99.95	100.24	99.85	99.25	99.57	99.17
	Cations per eight oxygens					
Si ----	2.161	1.98	2.083	2.031	1.957	2.128
Ti ----	-	-	-	-	-	-
Al ----	1.811	2.032	1.938	1.95	2.017	1.808
Fe ----	0.009	0.004	0.012	0.005	0.017	0.004
	3.981	4.016	0.033	3.986	3.991	3.940
Ca ----	0.845	0.960	0.893	0.984	1.021	0.982
Na ----	0.214	0.049	0.034	0.047	0.04	0.084
K -----	0.003	0.001	0.002	-	-	0.001
	1.062	1.08	0.929	1.031	1.061	1.067
mole % An	79.5	95.0	96.1	95.4	96.2	92.0
Ab	20.2	4.9	3.7	4.6	3.8	7.9
Or	0.3	0.2	0.2	-	0.1	

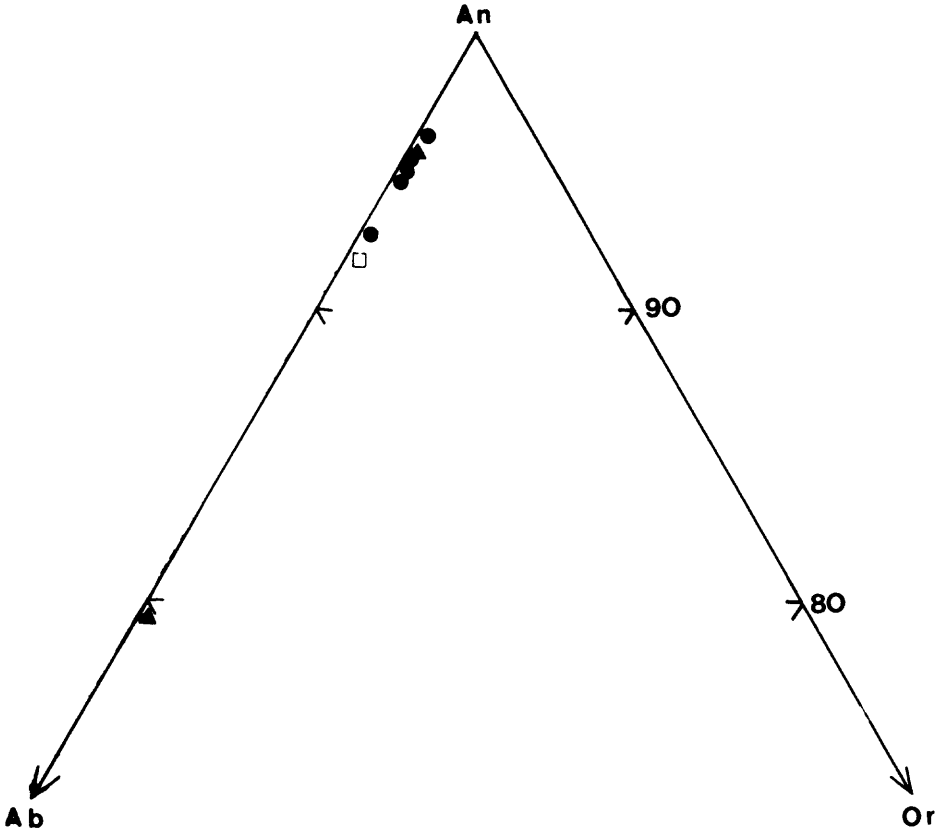

Figure 28.--Ternary plot of plagioclase compositions in the system An-Ab-Or. Closed circles=wehrlitic series; closed triangles=lherzolitic series, open square is plot of foliated hornblende gabbro.

Table 5. Electron probe analyses of hornblende

	Lherzolitic				Wehrlitic
Sample	6TNC	123BTNC	93TNC	121TNC	KG187
SiO_2 ---	45.26	55.55	44.98	45.56	46.83
TiO_2 ---	0.82	0.16	0.91	0.30	0.35
Al_2O_3 --	11.53	3.93	10.57	11.88	11.86
Cr_2O_3 --	0.05	0.46	0.07	0.05	0.08
FeO* ---	7.83	4.88	8.02	9.49	10.27
MnO ----	0.16	0.71	0.49	0.16	0.77
MgO ----	17.31	21.90	17.51	16.48	16.11
CaO ----	12.12	12.72	12.94	11.60	11.73
Na_2O ---	1.72	0.54	1.20	1.27	1.46
K_2O ---	-	0.04	0.30	-	0.26
Total	96.80	100.89	96.99	96.79	99.72
Fe^{3+} Corrected hornblende formulae based on 23 oxygens					
Si -----	6.404	6.412	6.426	6.494	6.494
Al -----	1.596	1.588	1.574	1.506	1.506
	8.000	8.000	8.000	8.000	8.000
Al -----	.326	.031	.205	.318	.434
Ti -----	.086	.015	.098	.037	.036
Cr -----	.008	.049	.008	.004	.009
Fe^{3+} ---	.874	.530	.690	.849	.881
Mg -----	.706	1.375	.999	.792	.640
	2.000	2.000	2.000	2.000	2.000
Mg -----	2.945	2.985	2.731	2.750	2.449
Fe^{2+} ---	.055	.015	.269	.250	.551
	3.000	3.000	3.000	3.000	3.000
Mn -----	.019	.081	.060	.019	.091
Ca -----	1.854	1.820	1.940	1.808	1.744
Na -----	.127	.099	--	.173	.165
	2.000	2.000	2.000	2.000	2.000
Ca -----	-	-	.043	-	-
Na -----	.343	.039	.332	.13	.229
K ------	-	.008	.057	-	.046
Mg* ----	.794	.874	.785	.760	.677
Ca/Ca+Na	.798	.938	.857	.856	.931
Ca/Ca+Na+K	.798	.934	.836	.856	.908

FeO* - total Fe as FeO
MG* = $Mg/Mg/Fe_T+Mn$

Table 6. Electron probe analyses of chromitic spinels

	Lherzolitic		
Sample	122TNC	122bTNC	103TNC
TiO_2 ----------	0.27	0.15	0.25
Al_2O_3 ----------	10.95	16.91	14.43
Cr_2O_3 ----------	52.87	46.19	42.50
V_2O_5 ----------	0.27	0.2	0.22
Fe_2O_3 ----------	5.81	7.12	12.3
FeO ----------	21.14	22.07	23.94
MnO ----------	0.59	0.64	0.64
MgO ----------	7.96	8.19	6.6
Total ----------	99.86	101.46	100.88
Formulae based on 24 cations			
Ti ----------	.054	.029	.051
Al ----------	3.46	5.129	4.504
Cr ----------	11.20	9.395	8.897
V ----------	.058	.041	.048
Fe^{3+} ----------	1.17	1.378	2.451
Total ----------	15.942	15.972	15.951
Fe^{2+} ----------	4.74	4.749	5.3
Mn ----------	.135	.14	.144
Mg ----------	3.181	3.14	2.606
Total ----------	8.056	8.029	8.050
Sp ----------	.219	.323	.284
Chr ----------	.708	.591	.561
Mag ----------	.074	.087	.157
$\frac{Fe+Mn}{Fe+Mn+Mg}$ --------	.665	.676	.762

Table 7. Electron probe analyses of spinels

	WEHRLITIC SERIES	LHERZOLITIC SERIES	
Sample	23TNC	201	93TNC
TiO_2 ----------	0.02	-	-
Al_2O_3 ----------	60.91	59.08	58.62
Cr_2O_3 ----------	-	2.03	1.08
V_2O_5 ----------	0.08	0.08	0.05
Fe_2O_3 ----------	8.06	5.07	7.31
FeO ----------	12.57	18.61	17.59
MnO ----------	0.08	0.08	0.05
MgO ----------	19.06	14.71	15.43
NiO ----------	-	-	-
Total ----------	100.78	99.66	100.13
Structural formula based on 24 cations			
Ti ----------	0.002	-	-
Al ----------	14.737	14.833	14.643
Cr ----------	-	0.341	0.181
V ----------	0.013	0.013	0.009
Fe^{3+} ----------	1.246	0.813	1.167
Total ----------	15.998	16.000	16.000
Fe^{3+} ----------	2.157	3.315	3.118
Mn ----------	0.015	0.015	0.009
Mg ----------	5.83	4.67	4.872
Ni ----------	-	-	-
Total ----------	8.002	8.000	7.999

Table 8. Electron probe analyses of magnetite

	Lherzolitic				Wehrlitic	
Sample	93STNC	93TNC	KG181	KG201	23TNC	67TNC
TiO_2 ----	0.05	3.77	1.92	2.46	4.59	2.04
Al_2O_3 ---	0.06	1.84	1.67	1.11	1.82	0.66
Cr_2O_3 ---	0.08	1.9	0.62	0.4	0.22	0.3
V_2O_5 ----	0.06	1.34	0.55	0.62	1.39	1.41
Fe_2O_3 ---	69.75	57.58	62.51	62.48	58.39	62.86
FeO -----	27.33	33.98	31.74	32.35	33.09	32.11
MnO -----	0.02	0.26	0.19	0.28	0.29	0.18
MgO -----	2.36	0.68	0.58	0.57	0.69	0.44
NiO -----	0.02	0.14	0.22	0.17	0.19	0.17
Total -	99.73	101.52	99.71	100.45	101.67	100.17
	Based on 24 cations					
Ti ------	0.011	0.843	0.438	0.561	1.018	0.468
Al ------	0.02	0.646	0.599	0.397	0.631	0.238
Cr ------	0.02	0.446	0.078	0.095	0.051	0.073
V -------	0.016	0.321	0.135	0.15	0.328	0.344
Fe^{3+} ----	15.923	12.885	14.311	14.236	12.953	14.41
Total -	15.99	15.141	15.561	15.439	14.981	15.533
Fe^{2+} ----	6.936	8.45	8.076	8.192	8.158	8.18
Mn ------	0.004	0.006	0.049	0.072	0.072	0.047
Mg ------	1.067	0.303	0.261	0.25	0.744	0.199
Ni ------	0.004	0.035	0.053	0.042	0.044	0.043
Total -	8.011	8.794	8.439	8.556	9.018	8.469
Sp ------	.001	.045	.040	.027	.045	.016
Chr -----	.001	.031	.005	.006	.004	.005
Mag + Usp	.998	.924	.955	.967	.951	.979
$\frac{Fe+Mn}{Fe+Mn+Mg}$	.956	.986	.991	.992	.970	.993

Table 8 (continued) Ilmenite

	Lherzolitic	Wehrlitic
	92TNC	65TNC
TiO_2	49.29	50.7
Al_2O_3	0.08	0.56
Cr_2O_3	0.07	-
V_2O_5	1.27	0.98
Fe_2O_3	-	-
FeO	47.99	44.81
MnO	2.50	2.14
MgO	0.18	1.17
NiO	0.11	-
Total	101.5	100.96
Formulae calculated on the basis of two cations		
Ti	.919	.937
Al	.002	.016
Cr	.001	-
V	.021	.016
Fe^{3+}	.096	.061
Fe^{2+}	.899	.860
Mn	.053	.045
Mg	.007	.065
Ni	.002	-
$\frac{Fe+Mn}{Fe+Mn+Mg}$	.993	.937
$FeTiO_3$	.852	.834
$MgTiO_3$	.007	.063
$MnTiO_3$	.050	.044
Fe_2O_3	.090	.059

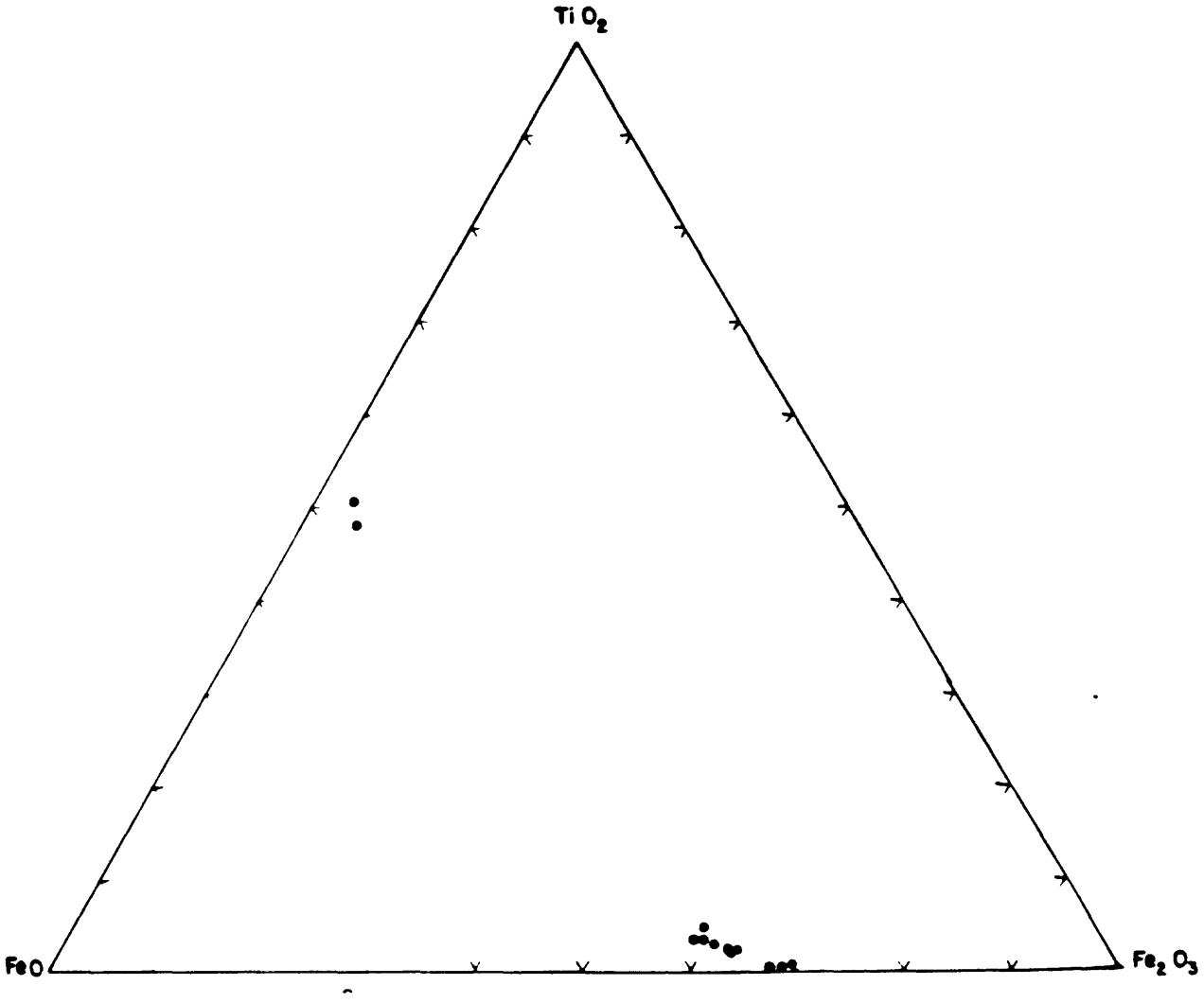

Figure 29.--The subsystem $FeO-Fe_2O_3-TiO_2$ showing compositions of analyzed magnetites and ilmenites. Diagram modeled after Carmicheal, Turner, and Verhoogen (1974, p. 279).

PETROLOGY

Whole-rock chemistry

Semiquantitative spectrographic analysis of 120 Tincup Peak whole rocks are shown in table 9. Ultramafic rocks of the lherzolitic series show higher MgO, MnO, and lower Al and Ca concentrations than the ultramafic rocks of the wehrlitic series.

Various oxides are plotted in an MgO variation diagram (fig. 30). The results show that the lherzolitic rocks are rich in Cr (modal chromite) and Ni (modal olivine). Vanadium in the wehrlitic series reaches highs of greater than 3,000 ppm (parts per million) in the rocks with more than average magnetite but never exceeds 700 ppm in the lherzolitic rocks. Strontium and barium show little difference between the two series.

Equilibration pressure and temperature

Equilibration occurred at low pressure based on the assumed stability of olivine+plagioclase. Both wehrlitic and lherzolitic rocks yield a temperature of 560°, log f_{O_2} $^{-22}$ from analyses of their FeTi oxide mineral pairs, using the Buddington and Lindsley (1964) equilibria diagram. No significant difference is observed because extensive subsolidus reequilibration occurred in both cases.

Crystallization models

Because evidence of cumulus processes is prominent in the Tincup Peak wehrlitic and lherzolitic rocks, fractional crystallization is assumed as an origin of each rock series. Primary minerals of the wehrlitic series crystallized in the sequence: olivine+clinopyroxene, magnetite (and accompanying Mg-Al spinel), hornblende, and plagioclase. This sequence produced the rock units wehrlite, olivine clinopyroxenite, magnetite clinopyroxenite, hornblende-magnetite clinopyroxenite, and hornblende gabbro. Mineral assemblages of lherzolitic rocks crystallized in the sequence: olivine, clinopyroxene, orthopyroxene, hornblende+magnetite (with spinel), and plagioclase. Resulting rock units were dunite-lherzolite, olivine-clinopyroxene heteradcumulate, olivine bronzite cumulates, and two-pyroxene gabbro. The increase in Ba and Sr and the decrease in Mg:(Mg+Fe) ratio through both rock series by fractionation of mafic minerals show variations that are common to stratiform intrusions such as the Stillwater and Bushveld complexes (Hess, 1960; Wager and Brown, 1968; Jackson, 1967). Vanadium shows a distinctive trend of enrichment, a maximum during cumulus magnetite crystallization, and a subsequent abrupt drop due to depletion in the liquid as a result of magnetite removal. The magnitude of the rise in vanadium content is far greater in the wehrlitic rock series than in the lherzolitic series.

Considering the crystallization history of the two Tincup Peak rock series, a modified schematic diagram from Kushiro (1972) may be used to illustrate the inferred crystallization paths of the nonplagioclase-bearing ultramafic rocks at Tincup Peak (fig. 31a). For any liquid whose composition falls in the stippled area D-Mg_2SiO_4-A, no reaction relationship occurs between olivine and liquid bulk composition X, for example, upon cooling will crystallize olivine driving the liquid toward the boundary curve AD. When it

Table 9. Semiquantitative spectrographic analyses

[N = not detected; L = detected, but below limit of determination; G = greater than value shown. Instrument: Wadsworth mounted, Jarrell-Ash, .5 m DC arc emission spectrograph]

Sample	Fe	Mg	Ca	Ti	Mn	B	Ba	Co	Cr	Cu	Ni	Sc	Sr	V
	(percent)				(ppm)									
Ultramafics/wenrlitic series														
3-77	15	7.	10.	.1	2,000	N	L	100	500	50	150	70	N	200
5-77	20	10.	2.	.1	2,000	N	L	200	150	50	300	50	N	150
9-77	20	7.	1.5	.3	2,000	N	30	200	500	700	200	50	N	1,000
10-77	10	5.	10.	.2	1,000	N	50	70	N	300	30	50	300	1,000
12-77	7	5.	10.	.07	700	N	30	50	150	30	100	20	300	70
14-77	15	7.	15.	.15	1,500	N	L	100	1,500	30	150	100	N	300
16-77	15	3.	15.	.15	700	N	300	20	200	1,500	20	20	700	200
22-77	20	7.	15.	.5	1,500	N	N	100	200	70	100	100	N	2,000
23-77	20	5.	5.	.7	1,500	N	L	150	100	70	200	70	N	5,000
26-77	15	7.	10.	.1	1,500	20	20	150	500	20	200	100	N	200
30-77	15	7.	7.	.05	1,500	50	20	100	300	30	150	50	100	150
34-77	15	10.	7.	.07	1,500	N	20	70	1,500	50	200	50	N	150
36-77	10	7.	10.	.1	1,500	N	L	70	2,000	100	200	50	N	200
42-77	15	7.	10.	.3	1,000	N	20	70	50	70	50	50	200	1,000
45-77	15	5.	7.	.2	1,000	N	L	70	N	15	30	7	300	500
47-77	7	7.	10.	.1	1,500	N	N	70	2,000	30	200	70	N	150
50-77	10	7.	10.	.07	1,500	N	20	100	2,000	15	200	70	L	200
51-77	10	7.	15.	.15	1,500	N	20	70	3,000	30	150	100	N	300
52-77	15	7.	7.	.5	1,500	N	N	70	300	500	50	100	L	1,000
54-77	15	5.	10.	.3	1,500	N	30	50	N	70	L	30	300	300
56-77	20	7.	5.	.5	1,500	N	20	100	200	1,500	150	70	N	3,000
57-77	15	7.	10.	.5	1,000	N	20	100	150	1,500	100	100	100	2,000
61-77	20	.7	.05	1.	1,500	N	20	150	5,000	70	150	15	N	5,000
62-77	15	5.	10.	.3	1,000	N	20	70	70	1,000	70	100	L	1,500
63-77	20	2.	1.5	.5	1,500	N	30	200	300	700	200	50	N	5,000
64-77	20	5.	10.	.5	1,000	N	L	100	500	500	100	100	N	3,000
66-77	15	10.	10.	.15	1,500	N	20	100	500	70	100	100	N	200
67-77	15	7.	15.	.15	1,000	N	L	100	1,500	70	150	100	N	200
68-77	15	5.	10.	.3	1,500	N	50	50	100	200	15	50	500	300
69-77	15	10.	10.	.15	2,000	N	20	100	500	50	100	70	N	200
70-77	20	5.	10.	.3	1,500	N	30	100	150	500	70	70	200	1,000
73-77	15	5.	10.	.3	1,500	N	20	70	100	700	70	100	100	1,000
74-77	15	7.	15.	.2	1,500	N	20	70	2,000	20	150	100	N	500
80-77	15	10.	15.	.1	1,000	N	N	70	1,500	500	150	70	N	200
90-77	15	7.	7.	.15	1,500	N	20	100	300	70	150	70	N	150
91-77	20	10.	.7	.05	1,500	N	L	200	50	100	300	20	N	50
116-77	15	7.	10.	.3	1,500	N	200	100	150	1,000	70	70	150	1,000
668-77	20	5.	10.	.3	1,000	N	L	100	500	500	70	100	N	1,500
94-77	20	10.	5.	.3	3,000	N	70	150	300	500	200	70	N	1,500
114-77	15	5.	10.	.1	2,000	30	20	70	150	10	50	50	200	500
115-77	15	3.	10.	.7	1,500	30	50	20	70	30	20	30	200	300
Ultramafics/lherzolitic series														
6-77	20	10.	2.	.1	1,500	N	20	150	150	70	300	50	N	200
7-77	15	7.	15.	.15	1,500	N	N	70	1,500	30	150	100	N	300
18-77	20	10.	.1	.01	700	70	L	500	300	2,000	1,000	10	N	20
19-77	15	7.	10.	.2	1,500	N	20	70	1,500	30	150	70	L	300
20-77	15	7.	5.	.02	1,500	N	L	100	2,000	100	500	15	N	30
21-77	15	10.	7.	.03	1,000	N	N	100	2,000	150	1,500	30	N	50
39-77	10	10.	.2	.015	700	N	N	150	5,000	N	1,500	7	N	20
44-77	10	7.	1.5	.05	1,000	N	N	70	2,000	50	300	20	N	70
46-77	10	10.	.3	.01	1,500	N	N	100	5,000	15	1,500	10	N	30
53-77	15	10.	2.	.03	1,500	N	N	150	500	50	500	30	N	70
58-77	15	10.	3.	.05	1,500	N	L	150	300	30	300	20	N	70
77-77	15	10.	.2	.015	2,000	100	N	100	3,000	L	1,000	10	N	50
79-77	15	10.	10.	.07	1,500	20	N	100	3,000	70	500	50	N	150
81-77	15	10.	.15	.015	1,000	N	N	150	5,000	200	1,000	15	N	50
88-77	15	10.	1.	.07	2,000	N	L	150	70	100	200	20	N	100
89-77	15	10.	1.	.1	2,000	N	30	150	100	70	200	30	N	150
123C-77	10	10.	.2	.00	1,000	N	N	100	5,000	7	1,500	5	N	30
40-77	15	7.	10.	.2	1,000	N	L	70	1,000	150	100	70	300	300
59-77	15	10.	10.	.07	1,000	N	N	70	5,000	30	300	50	L	100
88-77	15	5.	15.	.3	1,500	20	20	100	100	300	50	70	500	500
93-77	20	10.	5.	.2	1,500	N	20	150	2,000	500	300	70	L	700
103-77	10	10.	.5	.015	1,000	20	N	100	G(5,000)	50	2,000	10	N	50
123D-77	7	7.	5.	.03	1,000	N	N	50	2,000	7	300	30	N	100

Table 9 (continued)

Sample	Fe	Mg	Ca	Ti	Mn	B	Ba	Co	Cr	Cu	Ni	Sc	Sr	V
	(percent)				(ppm)									
Gabbroic rocks/wehrlitic series														
11-77	15	3.	10.	.2	1,000	N	30	50	N	150	5	30	500	300
13-77	20	5.	10.	.5	1,500	N	50	70	N	300	30	50	300	700
15-77	20	5.	10.	.5	1,500	N	150	100	N	200	20	100	300	1,000
25-77	15	3.	15.	.3	2,000	20	30	70	50	300	30	50	300	500
41-77	15	2.	10.	.3	1,000	N	20	70	L	70	10	50	300	300
43-77	15	5.	10.	.2	1,000	N	30	50	N	10	20	20	300	500
72-77	10	5.	15.	.2	1,000	N	30	50	100	50	30	50	500	300
75-77	10	3.	10.	.2	1,000	N	L	15	N	30	10	70	300	300
76-77	15	3.	10.	.3	2,000	N	L	20	L	100	10	50	300	200
83-77	15	7.	1.5	.3	2,000	N	20	70	300	1,500	150	50	L	700
84-77	15	5.	10.	.2	1,500	N	L	70	100	300	30	50	200	700
96-77	10	5.	10.	.07	1,000	N	20	70	300	100	100	30	150	150
97-77	7	5.	10.	.07	1,000	N	L	50	500	20	100	30	150	150
98-77	10	3.	10.	.2	1,000	N	50	50	70	30	30	50	500	300
99-77	15	3.	10.	.2	700	N	30	50	N	100	50	30	500	700
100-77	15	5.	7.	.2	1,500	N	L	50	200	50	50	70	200	300
101-77	15	3.	10.	.5	1,500	N	30	50	N	150	15	30	300	500
105-77	3	3.	10.	.03	700	20	150	20	150	20	30	30	300	70
111-77	15	5.	10.	.2	1,000	N	L	70	N	70	30	30	300	700
118B-77	15	5.	10.	.3	1,500	N	20	70	N	100	5	70	200	700
2-77	15	7.	10.	.2	1,500	N	20	70	700	500	70	70	300	300
55-77	15	3.	10.	.3	1,000	N	50	50	N	150	N	30	500	300
110-77	10	5.	15.	.1	700	N	20	70	70	10	50	5	500	200
117-77	5	5.	15.	.1	1,000	N	200	20	200	50	50	30	300	100
Gabbroic rocks/lherzolitic series														
1-77	10	5.	10.	.2	2,000	N	70	50	50	150	30	50	300	500
24-77	15	5.	10.	.3	1,500	30	100	70	50	150	20	50	700	300
27-77	15	5.	10.	.2	2,000	L	20	70	150	70	30	70	300	500
28-77	15	5.	10.	.2	1,500	20	20	70	150	1,000	50	50	300	700
29-77	15	5.	10.	.5	2,000	50	50	70	100	300	30	70	300	700
31-77	10	5.	10.	.1	1,500	20	L	70	200	20	100	50	150	200
33-77	7	5.	7.	.07	1,500	N	L	50	700	30	100	50	100	150
35-77	10	5.	10.	.1	1,500	N	L	50	500	50	100	50	100	200
37-77	7	7.	10.	.1	1,500	N	N	50	1,000	15	70	50	L	150
49-77	10	7.	10.	.05	1,500	N	20	70	300	5	100	50	150	150
92-77	15	7.	7.	.2	2,000	N	20	70	150	150	50	70	200	700
95-77	15	5.	10.	.2	1,500	N	20	50	N	150	15	50	300	500
106-77	15	5.	10.	.3	2,000	N	30	70	150	300	30	70	200	300
119-77	15	5.	10.	.3	1,500	N	L	50	150	200	20	70	200	500
107-77	15	5.	15.	.2	2,000	20	30	70	70	300	30	50	500	700
Felsic rocks not belonging to either series														
8-77	15	5.	15.	.3	1,500	N	50	50	50	300	10	50	500	500
17-77	1	.7	1.5	.05	500	N	150	L	N	20	10	5	150	20
32-77	3	2.	7.	1.	1,000	L	150	10	10	L	15	15	700	70
38-77	15	5.	10.	.2	1,500	N	L	50	50	20	20	70	300	500
48-77	7	.15	.1	.003	20	N	N	5	N	300	10	N	N	15
60-77	2	5.	10.	.05	700	N	20	20	300	20	100	30	100	100
78-77	15	7.	10.	.1	1,000	N	30	70	200	100	100	50	200	200
85-77	3	.05	.3	.01	20	N	20	10	N	150	15	N	L	10
82-77	15	3.	3.	.3	1,500	N	100	30	100	20	30	30	300	300
86-77	15	3.	7.	.3	1,500	30	200	50	50	30	7	30	500	200
87-77	1	.7	20.	.02	300	30	20	5	N	10	7	5	L	50
102-77	2	.7	1.5	.1	700	30	150	2	N	20	7	7	L	30
113-77	7	2.	3.	.2	1,500	N	100	10	70	30	20	30	200	200

*Analyses by David Grimes.

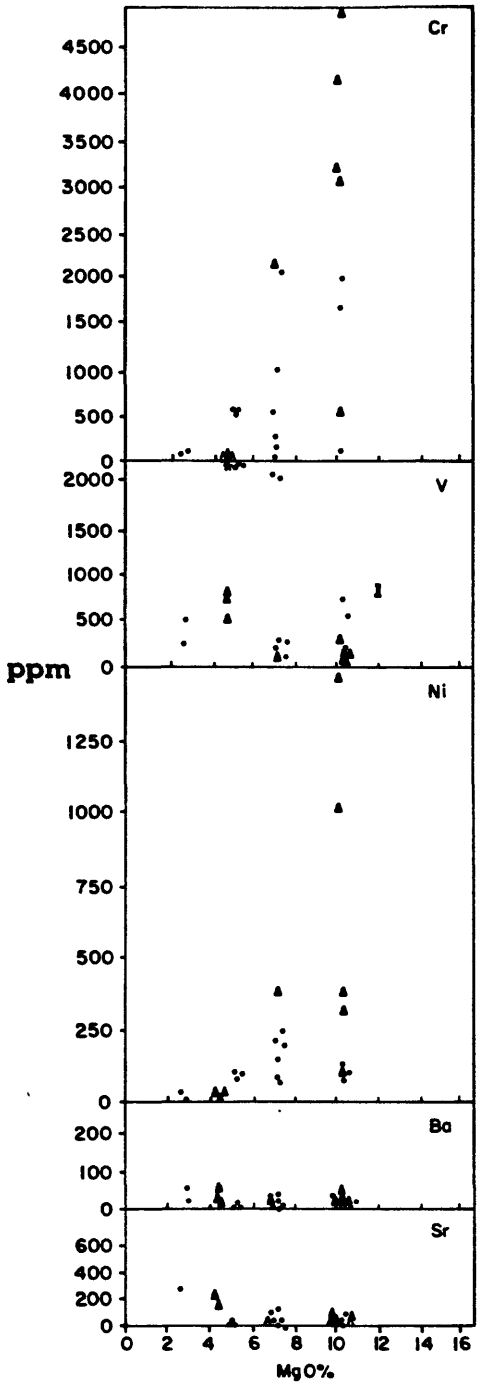

Figure 30.--Variation diagram showing plots of Sr, Ba, Ni, V, and Cr versus MgO percent. Closed circles = wehrlitic series; closed triangles = lherzolitic series.

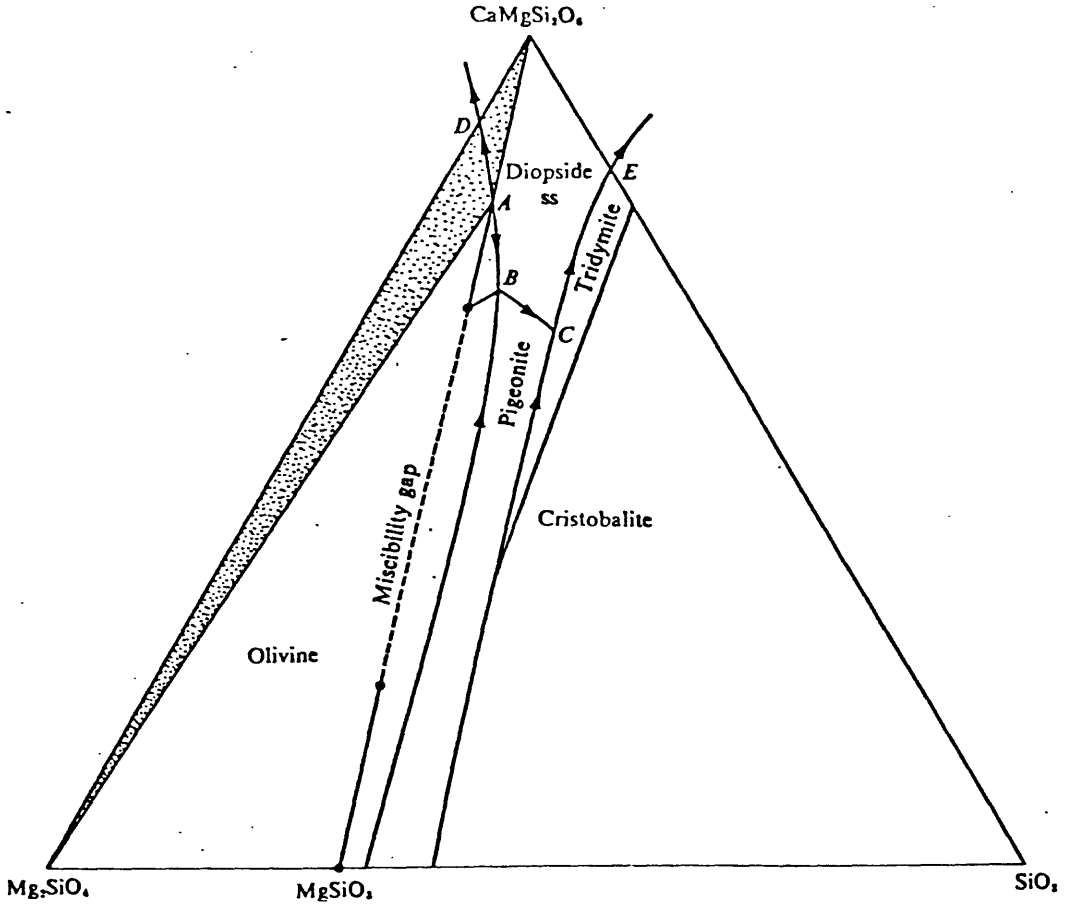

Figure 31.--(a) The system Mg_2SiO_4-$CaMgSi_2O_6$-SiO_2 at 1 bar (after Kushiro, 1972). Liquids in the stippled area approximate the crystallization sequence of the wehrlitic series. Bulk compositions close to X approximate the crystallization sequence inferred for lherzolitic series rocks.

reaches AD, a diopside solid solution precipitates. This crystallization sequence is analogous to that derived from the Tincup Peak wehrlitic series. Alternatively, liquid compositions falling within the area Mg_2SiO_4-A-B-Mg_2SiO_3 will display an olivine-liquid reaction relationship and may be said to represent the tholeiitic magma type (Carmichael and others, 1974). Rocks generated from liquids fractionally crystallizing in this field approximate those observed in the lherzolitic series.

Systems involving plagioclase are shown in figure 31b (after Irvine, 1974). The diagram shows the inferred liquidus differentiation paths of suggested bulk compositions of wehrlitic (U) and lherzolitic (P) rocks which are alkaline (critically undersaturated) and subalkaline respectively. The paths are derived mainly from petrographic textural evidence; however, mineral and rock chemistry substantiate the suggested model. Point C on the olivine-clinopyroxene liquidus boundary marks the thermal divide separating the differentiation paths of the two melt compositions. Following the crystallization paths, bulk compositions U and P produce mineral assemblages that are broadly analogous in their crystallization sequence and rock paths observed in the Tincup Peak wehrlitic and lherzolitic series rocks, respectively.

Economic geology

Location and geologic setting of magnetite deposit

The Tincup Peak magnetite deposit is located in the eastern part of the mapped area. Low-grade ore (60 percent Fe, 1.4 percent TiO_2, 0.18 percent Cr_2O_3) is exposed within the ultramafic rocks in the area between Gold Basin and Gate Saddle.

The magnetite deposit occurs in a lenticular sill-like body of clinopyroxene-rich rocks. The body is approximately 0.8 km wide (east west) and at least 2 km long (north-northeast) and is conformable in orientation to the igneous layering within the ultramafic unit. The clinopyroxene-rich ultramafic unit is bounded on the east by a partially obscured east-dipping thrust. The thrust contact is irregularly intruded by a dike of pegmatitic hornblende gabbro approximately 11.5 to 16 m wide.

On the western margin, the ultramafic unit is in intrusive contact with hornblende gabbro.

The predominant rock types in the border zone of ultramafic body are wehrlite and olivine clinopyroxenite. These rocks grade into hornblende-bearing clinopyroxenites and eventually into hornblende magnetite clinopyroxenites toward the center of the unit. Contacts are irregular and transitional between rock units.

The main ore zone is approximately 800 m long and 250 m wide (maximum). The ore has an ill-defined zonal distribution based on modal amounts of magnetite. This crudely defined arrangement is displayed in figure 32 as three gradational zones of magnetite concentration. The inner (core) zone contains 30 to 65 percent oxides, the aggregate zone 10 to 35 percent, and the outer zone contains accessory to slightly greater than accessory amounts of magnetite. The highest grade ores are layered and trend N. 70° E., dipping steeply to the northwest.

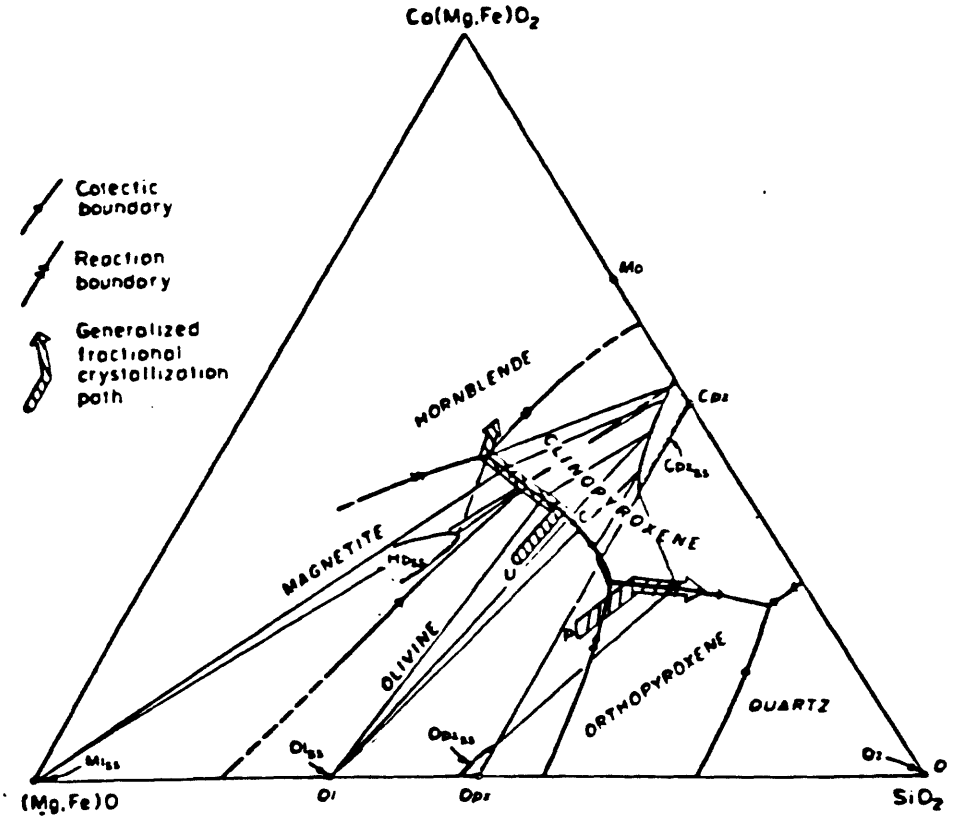

Figure 31.—(b) Schematic phase diagram model, after Irvine (1974), contrasting the liquidus differentiation paths of the parent liquids of the wehrlitic (u) and lherzolitic (p) series rocks. The phase boundaries are projected from the compositional points of plagioclase, water, and magnetite; to show a field for magnetite it is assumed that when this mineral was forming the system was buffered with respect to oxygen, consequently its effect on the liquidus path is determined by projecting its composition from oxygen to the apex (Mg, Fe) O, as shown. Point C on the olivine clinopyroxene liquidus boundary marks the thermal divide separating the differentiation paths of alkaline (critically undersaturated) and the more siliceous, subalkaline melts.

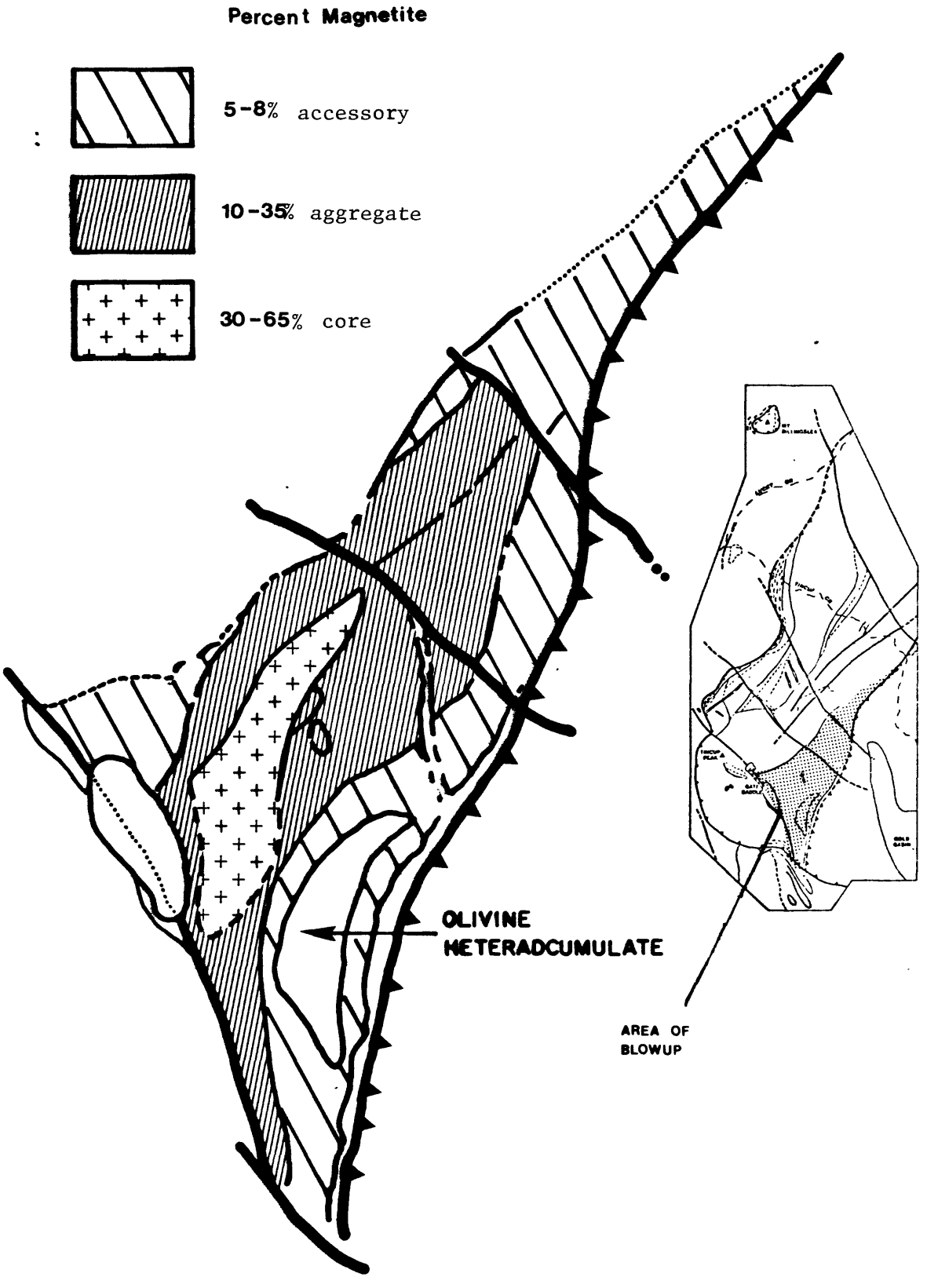

Figure 32.--Map showing schematic zonation of magnetite concentrations. Inset shows location of blowup.

The principal mineral components of the ore are invariably magnetite, hercynitic spinel, and ilmenite, commonly in that order of abundance. Magnetite in reflected light occurs as optically homogeneous grains with rare sandwich laths (intergrowths of thick lamallae) of ilmenite. Spinel occurs as discrete anhedral grains.

Geochemistry

Figure 33 shows the areal distribution of geochemical anomalies in the Tincup area. In the ore body itself, in addition to high values of iron, vanadium reaches 2,000 to 3,000 ppm in the core region of the clinopyroxenite body. Values of 1,000 to 2,000 ppm Ni are also observed, associated with large fragments of lherzolitic rocks in the area. The chromium anomaly represents finely disseminated chromite grains in dunite. Small amounts of chromite also occur in thin layers in dunite.

Copper anomalies, mainly disseminated chalcopyrite, occur in fractured rock associated with faulting and veining near a granitic pluton in the southern portion of the area.

Geophysical studies

A ground-based magnetometer survey was conducted to try to develop a means of interpreting the intrusive features of the deposit (fig. 34). The traverses taken to construct the map are shown in the inset. Magnetic highs show that the distribution of concentrated magnetite follows a northeast to southwest orientation. The form of the contours reflect the strike lines of the elongated sill-like body. The pattern and intensity of magnetization in the Tincup Peak area is similar to that shown in the aeromagnetic map of the Kerby and part of the Grants Pass quadrangles (Balsley and others, 1960).

Ore genesis

Postemplacement faulting and late intrusion of the hornblende gabbro has undoubtedly destroyed some of the evidence that could be used in discussions concerning the genesis of the magnetite deposit at Tincup Peak and enclosing rocks. However, the preservation of primary igneous layering, size-graded bedding, and original cumulus textures indicate an igneous origin for the enclosing rocks as well as the orebody itself.

Crystallization of olivine and clinopyroxene appear to have preceded that of magnetite. Magnetite was followed by hornblende and plagioclase in the crystallization sequence. The distribution of magnetite ore, both as a component in cyclic layers (polymineralic) or as discrete layers (near monomineralic) conformable to the dominant layering in the wehrlitic body can be explained by processes apparently controlled by fractional crystallization and gravity setting.

SUMMARY

The Tincup Peak ultramafic-mafic complex consists of two separate rock series, wehrlitic and lherzolitic, that show evidence of cumulus fractional crystallization from two types of magma. Neither series shows characteristics indicative of Alpine type "tectonite" ultramafics, i.e., high-temperature

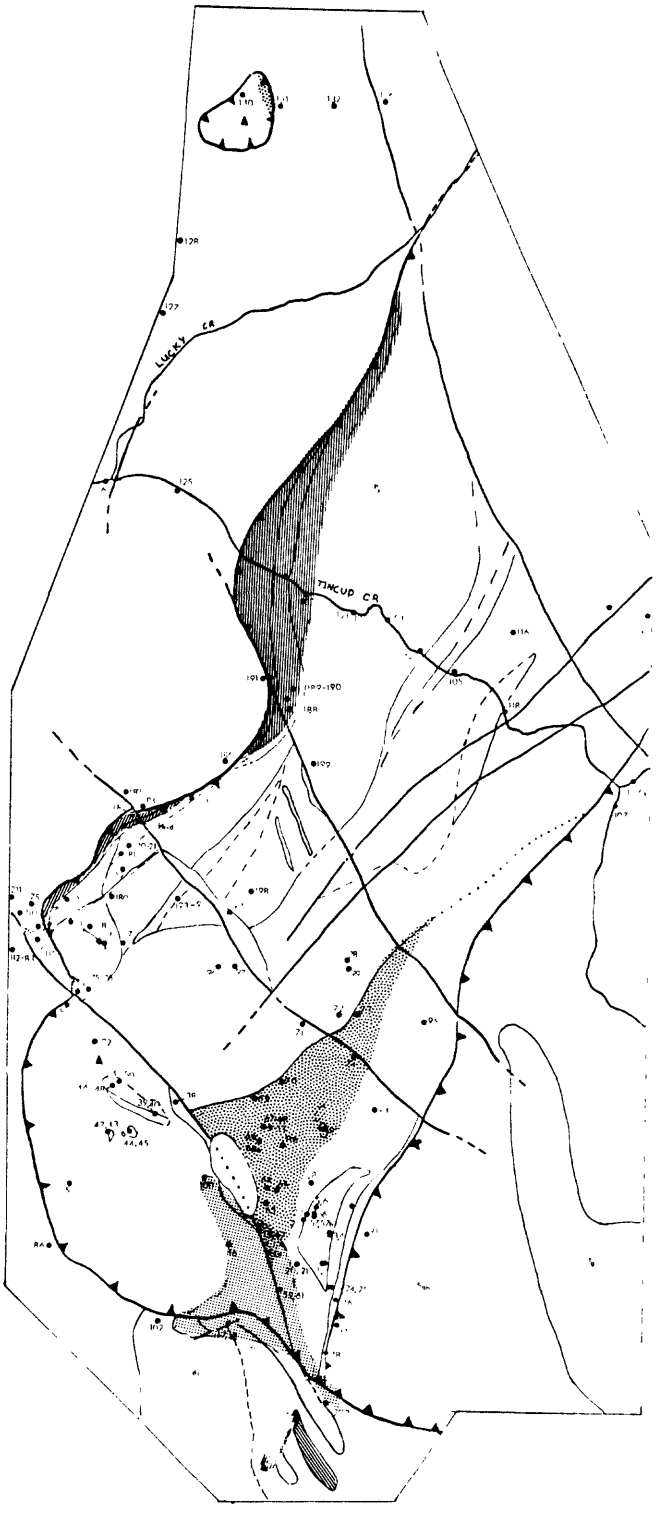

Figure 33.--Map showing anomalous concentrations of metals based on semiquantitative spectrographic rock analyses. Stripe pattern = chromium; coarse-stippled pattern = vanadium; fine-stippled pattern = copper.

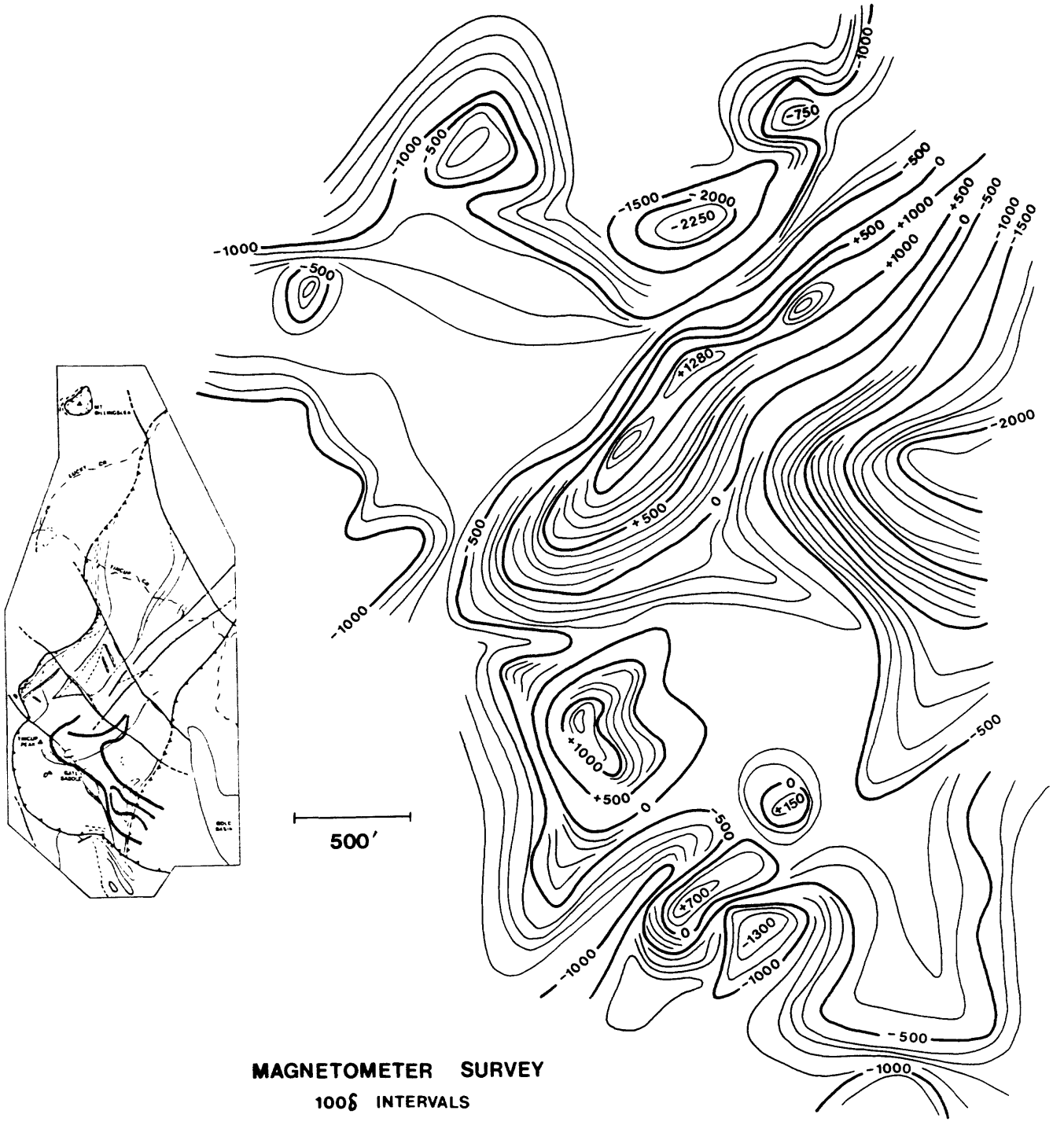

Figure 34.--Interpretive contour map of Tincup Peak area. Contour intervals are 100 gammas. Traverses were designed to trend across the stike of various units and are shown in inset. Inset also shows outline of ore body as in Figure 32.

crystal deformation or restricted magnesian composition. The wehrlitic rocks of Tincup Peak, instead, seem similar to alkaline magmas found in the zoned ultramafic complexes of southeastern Alaska (Irvine, 1974; Ruckmick and Noble, 1959). Lherzolitic series rocks resemble those of tholeiitic stratiform ultramafic complexes and ophiolitic cumulates (see Coleman, 1977, p. 35-47).

Primary layering, S_1, is the oldest structural-stratigraphic feature of the Tincup ultramafic-mafic complex. The complex was thrust westward over an older foliated hornblende gabbro terrain. The westward overriding thrusts and westward outlying klippe, Mount Billingslea, are characteristic structural features of pre-Tertiary Klamath Mountain terrain.

Ultramafic-gabbro rocks from the wehrlitic series indicate that the following rock types crystallized: wehrlite, olivine clinopyroxenite, magnetite clinopyroxenite, magnetite hornblende clinopyroxenite, and hornblende gabbro. Crystallization of lherzolitic rocks produced the rock sequence: dunite-lherzolite, olivine clinopyroxene heteradcumulate, olivine bronzite cumulates, and two-pyroxene gabbro. Principal differences in these two rock series lie in their systematic grain size difference, the sequential crystallization of the minerals clinopyroxene-magnetite-hornblende in the wehrlitic series versus olivine-clinopyroxene-orthopyroxene in lherzolitic rocks, and Ni and V variations.

Mineral chemistry and oxide variation diagrams show clear fractionation trends from olivine-rich ultramafic rocks to gabbroic rocks with abundant plagioclase.

The magnetite ore deposit, with clear magmatic affinites, forms an area about 800 m long by 250 m wide (maximum) and has a vertical extent of approximately 70 m. The ore ranges from 10 to 65 percent oxide minerals.

REFERENCES

Albee, A. L., and Ray, L., 1970, Correction factors for electron-probe microanalysis of silicates, oxides, carbonates, phosphates and sulfates: Analytical Chemistry, v. 42, p. 1408-1414.

Bailey, E. H., and Blake, M. C., Jr., 1974, Major chemical characteristics of Mesozoic Coast Range ophiolite in California: U.S. Geological Survey Journal of Research, v. 2, no. 6, p. 637-656.

Bailey, E. H., Blake, M. C., Jr., and Jones, D. L., 1970, On-land Mesozoic oceanic crust in California Coast Ranges, in Geological Survey research 1970: U.S. Geological Survey Professional Paper 700-C, p. C70-81.

Baldwin, E. M., 1969, Thrust faulting along the lower Rogue River, Klamath Mountains, Oregon: Geological Society of America Bulletin, v. 80, no. 10, p. 2047-2052.

Balsley, J. R., Bromery, R. W., Remington, E. W., and others, 1960, Aeromagnetic map of the Kerby and part of the Grants Pass quadrangles, Josephine and Curry Counties, Oregon: U.S. Geological Survey Geophysical Investigations Map GP-197, scale 1:96,000.

Bence, A. E., and Albee, A. L., 1968, Empirical correction factors for the electron microanalysis of silicates and oxides: Journal of Geology, v. 76, p. 382-403.

Blake, M. C., Jr., 1969, Blueschist facies metamorphism related to regional thrust faulting: Tectonophysics, no. 8, p. 237-246.

Blake, M. C., Jr., Irwin, W. P., and Coleman, R. G., 1967, Upside-down metamorphic zonation, blueschist facies, along a regional thrust in California and Oregon, in Geological Survey research 1967: U.S. Geological Survey Professional Paper 575-C, P. C1-C9.

Buddington, A. F., and Lindsley, D. H., 1964, Iron-titanium oxide minerals and synthetic equivalents: Journal of Petrology, v. 5, p. 310-357.

Carmichael, I. S. E., Turner, F. J., and Verhoogen, J., 1974, Igneous petrology: New York, McGraw-Hill, 739 p.

Challis, G. A., 1965, The origin of New Zealand ultramafic intrusions: Journal of Petrology, v. 6, p. 322-364.

_____1966, The genetic position of "alpine-type" ultramafic rocks: Volcanology Bulletin, v. 29, p. 283-302.

Coleman, R. G., 1977, Ophiolites: Ancient oceanic lithosphere?: New York, Springer-Verlag.

Davis, G. A., 1963, Structure and mode of emplacement of Caribou Mountain pluton, Klamath Mountains, California: Geological Society of America Bulletin, v. 74, no. 3, p. 331-348.

_____1964, Regional Mesozoic thrusting in the south-central Klamath Mountains of California [abs.]: Geological Society of America Abstracts with Programs, Annual Meeting, Seattle, Wash., p. 28.

_____1968, Westward thrust faulting in the south-central Klamath Mountains, California: Geological Society of America Bulletin, v. 79, no. 7, p. 911-934.

_____1969, Tectonic correlations, Klamath Mountains and western Sierra Nevada, California: Geological Society of America Bulletin, v. 80, no. 6, p. 1095-1108.

Dick, H. J. B., 1976, The origin and emplacement of the Josephine peridotite of southwestern Oregon: New Haven, Connecticut, Yale University, Ph. D. thesis, 409 p.

Diller, J. S., 1902, Topographic development of the Klamath Mountains: U.S. Geological Survey Bulletin 196, 69 p.

_____1914, Mineral resources of southwest Oregon: U.S. Geological Survey Bulletin 546, 147 p.

Diller, J. S. and Kay, G. F., 1924, Description of the Riddle quadrangle [Oregon]: U.S. Geological Survey, Geologic atlas of the United States, Riddle folio, Oregon (no. 218), 8 p.

Dott, R. H., Jr., 1965, Mesozoic-Cenozoic tectonic history of the southwestern coast in relation to Cordilleran orogenesis: Journal of Geophysical Research, v. 70, no. 18, p. 4687-4707.

_____1971, Geology of the southwestern Oregon coast west of the 124th meridian: Oregon Department of Geology and Mineral Industries Bulletin 69, 63 p.

Findlay, D. C., 1969, Origin of the Tulameen ultramafic-gabbro complex, southern British Columbia: Canadian Journal of Earth Sciences, v. 6, p. 399-425.

Green, D. H., 1964, The petrogenesis of the high-temperature peridotite intrusion in the Lizard Area, Cornwall: Journal of Petrology, v. 5, p. 131-188.

Haggerty, S. E., and Baker, I., 1967, The alteration of olivine in basaltic and associated lavas. Part I. High temperature alteration: Contributions to Mineralogy and Petrology, v. 16, p. 233.

Hess, H. H., 1960, Stillwater igneous complex, Montana, a quantitative mineralogical study: Geological Society of America Memoir 80, 225 p.

Himmelberg, G. R., and Coleman, R. G., 1968, Chemistry of primary minerals and rocks from the Red Mountain-Del Puerto ultramafic mass, California, in Geological Survey research 1968: U.S. Geological Survey Professional Paper 600-C, p. C18-C26.

Hotz, P. E., 1971, Plutonic rocks of the Klamath Mountains, California and Oregon: U.S. Geological Survey Professional Paper 684-B, 20 p.

Irvine, T. N., 1959, The ultramafic complex and related rocks of Duke Island, southeastern Alaska: Pasadena, California Institute of Technology, Ph. D. thesis, 320 p.

_____1963, Origin of the ultramafic complex at Duke Island, southeastern Alaska: Mineralogical Society of America Special Paper, p. 36-45.

_____1967, The Duke Island ultramafic complex, southeastern Alaska in Wyllie, P. J. ed., Ultramafics and related rocks: New York, John Wiley, p. 84-97.

_____1973, Bridget cove volcanics, Juneau area, Alaska: Possible parental magma of Alaskan-type ultramafic complexes: Carnegie Institute Washington Year Book 72, p. 478-491.

_____1974, Petrology of the Duke Island ultramafic complex, southeastern Alaska: Geological Society of America Memoir 138, 240 p.

Irwin, W. P., 1964, Late Mesozoic orogenies in the ultramafic belts of northwestern California and southwestern Oregon: U.S. Geological Survey Professional Paper 501-C, p. C1-9.

_____1966, Geology of the Klamath Mountains province, in Geology of northern California: California Division of Mines and Geology Bulletin 190, p. 19-38.

Jackson, E. D., 1961, Primary textures and mineral associations in the ultramafic zone of the Stillwater complex, Montana: U.S. Geological Survey Professional Paper 358, 106 p.

_____1967, Ultramafic cumulates in the Stillwater, Great Dyke, and Bushveld intrusions, in Wyllie, P. J., ed., Ultramafics and related rocks: New York, John Wiley, p. 20-38.

Jackson, E., D., and Thayer, T. P., 1972, Some criteria for distinguishing between stratiform, concentric, and alpine peridotite-gabbro complexes: 24th International Geologic Congress, Montreal, sec. 2, p. 289-296.

Jorgenson, D. B., 1970, Petrology and origin of the Illinois River gabbro, a part of the Josephine peridotite-gabbro complex, Klamath Mountains, southwestern Oregon: Santa Barbara, University of California, Ph. D. thesis, 226 p.; Dissertation Abstracts, v. 31, no. 6, p. 3482.

_____1971, Origin of patchy zoning in plagioclase from gabbroic rocks of southwestern Oregon: Geological Society of America Bulletin, v. 82, no. 9, p. 2667-2670.

Kays, M. A., 1970, Mesozoic metamorphism, May Creek Schist belt, Klamath Mountains, Oregon: Geological Society of America Bulletin, v. 81, no. 9, p. 2743-2758.

Kushiro, I., 1972, Determination of liquidus relations in synthetic silicate systems with electron probe analysis: The system forsterite-diopside-silica at 1 atmosphere: American Mineralogy, v. 57, p. 1260-1271.

Loney, R. A., and Himmelberg, G. R., 1977, Geology of the gabbroic complex along the northern border of the Josepine peridotite, Vulcan Peak area, southwestern Oregon: U.S. Geological Survey Journal of Research, v. 5, no. 6, p. 761-781.

Loney, R. A., Himmelberg, G. R., and Coleman, R. G., 1971, Structure and petrology of the alpine-type peridotite at Burro Mountain, California: Journal of Petrology, v. 12, p. 245-309.

Medaris, L. G., Jr., and Dott, R. H., Jr., 1970, Mantle-derived peridotites in southwestern Oregon: Relation to plate tectonics: Science, v. 169, p. 971-974.

Mossman, D. J., 1973, Geology of the Greenhills ultramafic complex, Bluff Peninsula, Southland, New Zealand: Geological Society of America Bulletin, v. 84, p. 39-62.

Nicolas, A., Bouchez, J. L., Boudier, F., and Mercier, J. G., 1971, Textures, structures, and fabrics due to solid state flow in some European lherzolites: Tectonophysics, v. 12, p. 55-86.

Page, N. J, 1967a, Serpentinization at Burro Mountain, California: Contributions to Mineralogy and Petrology, v. 14, p. 321-342.

_____1967b, Serpentinization in a sheared serpentinite lens, Tiburon Peninsula, California, in Geological Survey research 1967: U.S. Geological Survey Professional Paper 600-B, p. 821-828.

Page, N. J; Gray, Floyd; Cannon, J. K.; Foose, Mike; Lipin, Bruce; Moring, B. C.; Nicholson, S. W.; Sawlin, M. G.; Till, Alison; and Ziemianski, W. P., 1980, Geologic map of the Kalmiopsis Wilderness: U.S. Geological Survey Miscellaneous Field Studies Map MF-1240A.

Pike, J. E. N., and Schwarzman, E. C., 1977, Classification of textures in ultramafic xenoliths: Journal of Geology, v. 85, p. 49-61.

Ramp, Lenin, 1957, Nature and origin of southwestern Oregon chromite deposits: Mining Engineering, v. 9, no. 8, p. 894-897.

_____1961, Chromite in southwestern Oregon: Oregon Department of Geology and Mineral Industries Bulletin 52, 169 p.

_____1969, Dothan(?) fossils discovered: The Ore Bin, v. 31, no. 12, p. 245-246.

_____1972, Geology and mineral resources of Douglas County, Oregon: Oregon Department of Geology and Mineral Industries Bulletin 75, 106 p., including map, scale 1:250,000.

_____1975, Geology and mineral resources of the upper Chetco drainage area, Oregon, including the Kalmiopsis Wilderness and Big Craggies Botanical areas: Oregon Department of Geology and Mineral Industries Bulletin 88, 47 p.

Ruckmick, J. C., and Noble, J. A., 1959, Origin of the ultramafic complex at Union Bay, southeastern Alaska: Geological Society of America Bulletin, v. 70, p. 981-1018.

Streckeisen, A. L., 1973, Classification and nomenclature of plutonic rocks: Neues Jahrbuch fur Mineralogie Monatshefte, v. 4, p. 149-164.

Taliaferro, N. L., 1942, Geologic history and correlation of the Jurassic of southwestern Oregon and California: Geological Society of America Bulletin, v. 53, no. 1, p. 71-112.

Wager, L. R., and Brown, G. M., 1968, Layered igneous rocks: San Francisco, W. H. Freeman, 588 p.

Walker, G. W., 1973, Preliminary geologic and tectonic map of Oregon east of the 121st meridian: U.S. Geological Survey Miscellaneous Field Studies Map MF-495, scale 1:5,000,000 and 1:1,000,000.

Wells, F. G., 1955, Preliminary geologic map of southwestern Oregon west of meridian 122° west, and south of parallel 43° north: U.S. Geological Survey Mineral Investigations Field Studies Map MF-38, scale about 1 in. to 4 mi.

Wells, F. G., Hotz, P. E., and Cater, F. W., 1949, Preliminary description of the geology of the Kerby quadrangle, Oregon: Oregon Department of Geology and Mineral Industries Bulletin, v. 40, 23 p.

Wells, F. G., and Peck, D. L., 1961, Geologic map of Oregon west of the 121st meridian: U.S. Geological Survey Miscellaneous Geologic Investigations Map I-325.

Wilshire, H. G., and Pike, J. E. N., 1975, Upper mantle diaprism: Evidence from analogous features in alpine peridotites and ultramafic inclusions in basalts: Geology, v. 3, p. 467-470.

Worst, B. G., 1960, The Great Dyke of southern Rhodesia: Rhodesia Geological Survey Bulletin 47, 239 p.

APPENDIX

APPENDIX

[See Sample Locality Map, page A-6]

Sample listing of rocks from the Tincup Peak area

Sample number	Rock name
1TNC77	Gabbro
2TNC77	Coarse gabbro
3TNC77	Pyroxenite
4TNC77	Hornblende gabbro-pegmatite
5TNC77	Olivine-rich wehrlite
6TNC77	Olivine pyroxene heteradcumulate
7TNC77	Olivine clinopyroxenite
8TNC77	Diabase dike
9TNC77	Altered pyroxenite
10TNC77	Wehrlite
11TNC77	Hornblende gabbro (pegmatite)
12TNC77	Troctolite
13TNC77	Hornblende gabbro with diabase dike contact
14TNC77	Olivine wehrlite
15TNC77	Hornblende gabbro
16TNC77	Altered serpentinized pyroxenite
17TNC77	Muscovite granite
18TNC77	Fault gauge
19TNC77	Altered lherzolite
20TNC77	Serpentinized dunite
21TNC77	Olivine-rich peridotite (altered)
22TNC77	Magnetite-hornblende clinopyroxenite
23TNC77	Magnetite-hornblende clinopyroxenite
24TNC77	Altered two pyroxene gabbro
25TNC77	Hornblende gabbro (mylonitized)
26TNC77	Coarse olivine-rich wehrlite
27TNC77	Two-pyroxene gabbro
28TNC77	Altered gabbro
29TNC77	Two-pyroxene gabbro
30TNC77	Olivine wehrlite
31TNC77	Two-pyroxene gabbro
32TNC77	Siliceous dikes
33TNC77	Two-pyroxene gabbro
34TNC77	Wehrlite
35TNC77	Gabbro
36TNC77	Olivine clinopyroxenite
37TNC77	Two-pyroxene gabbro
38TNC77	Foliated gabbro
39TNC77	Serpentinized dunite
40TNC77	Two-pyroxene gabbro

Sample number	Rock name
41TNC77	Hornblende gabbro
42TNC77	Troctolite
43TNC77	Hornblende gabbro with fine-grained inclusion
44TNC77	Dunite inclusion in troctolite
45TNC77	Troctolite
46TNC77	Dunite
47TNC77	Wehrlite
48TNC77	Quartz dike
49TNC77	Altered two-pyroxene gabbro
50TNC77	Clinopyroxenite
51TNC77	Clinopyroxenite
52TNC77	Clinopyroxenite
53TNC77	Dunite with pyroxenite clusters
54TNC77	Hornblende gabbro
55TNC77	Hornblende gabbro with xenoliths of pyroxenite
56TNC77	Hornblende-magnetite pyroxenite
57TNC77	Magnetite clinopyroxenite
57BTNC77	Clinozoisite
58TNC77	Olivine-clinopyroxene heteradcumulate
59TNC77	Dunite
60TNC77	Altered gabbro
61TNC77	Magnetite ore
62TNC77	Olivine clinopyroxenite
63TNC77	Hornblende-magnetite clinopyroxenite
64TNC77	Hornblende-magnetite clinopyroxenite
65TNC77	Hornblende-magnetite clinopyroxenite
66TNC77	Hornblende-magnetite clinopyroxenite
67TNC77	Hornblende-magnetite clinopyroxenite
69TNC77	Hornblende-magnetite clinopyroxenite
70TNC77	Troctolite
71TNC77	Olivine gabbro
72TNC77	Hornblende gabbro
73TNC77	Altered pyroxenite
74TNC77	Clinopyroxenite
75TNC77	Foliated hornblende gabbro
76TNC77	Foliated hornblende gabbro
77TNC77	Dunite
78TNC77	Diorite
79TNC77	Dunite peridotite
80TNC77	Pyroxenite
81TNC77	Contact specimen; dunite with pyroxenite
82TNC77	Fine-grained gneiss
83TNC77	Altered gabbro
84TNC77	Hornblende
85TNC77	Felsic dike

Sample number	Rock name
86TNC77	Diabasic dike
87TNC77	Aplite
88TNC77	Olivine-clinopyroxene heteradcumulate
88BTNC77	Olivine-clinopyroxene heteradcumulate
89TNC77	Olivine-clinopyroxene heteradcumulate
90TNC77	Olivine clinopyroxenite
91TNC77	Wehrlite
92TNC77	Two-pyroxene gabbro
93TNC77	Olivine-clinopyroxene heteradcumulate
94TNC77	Magnetite-hornblende clinopyroxenite
95TNC77	Two-pyroxene gabbro
96TNC77	Hornblende gabbro
97TNC77	Hornblende gabbro
98TNC77	Hornblende gabbro
99TNC77	Hornblende gabbro
100TNC77	Altered gabbro
101TNC77	Hornblende-gabbro pegmatite
102TNC77	Muscovite granite
103TNC77	Dunite
104TNC77	Pyroxenite
105TNC77	Hornblende gabbro
106TNC77	Two-pyroxene gabbro
107TNC77	Two-pyroxene gabbro
110TNC77	Hornblende gabbro
111TNC77	Two-pyroxene gabbro with xenoliths in hornblende gabbro
112TNC77	Dunite
113TNC77	Foliated gabbro
114TNC77	Pyroxenite
115TNC77	Pyroxenite
116TNC77	Foliated dike with pyroxenite
117TNC77	Hornblende gabbro
118TNC77	Two-pyroxene gabbro
118BTNC77	Hornblende gabbro
119TNC77	Two-pyroxene gabbro
120TNC77	Foliated gabbro
121TNC77	Lherzolite
122TNC77	Dunite
123ATNC77	Two-pyroxene gabbro
123BTNC77	Layered lherzolite
123CTNC77	Layered lherzolite

Sample number	Rock name
123DTNC77	Pyroxenite
78KG106	Amphibolite schist
78KG113	Altered gabbro
78KG114	Gossan
78KG115	Epidotized gabbro
78KG116	Altered gabbro
78KG118	Hornblende gabbro with wehrlite inclusion
78KG119	Pyroxenite
78KG120	Serpentinite
78KG121	Gneissic amphibolite
78KG122	Dunite
78KG123	Dunite-lherzolite
78KG124	Hornblende-magnetite clinopyroxenite
78KG125	Foliated hornblende gabbro
78KG126	Foliated hornblende gabbro
78KG126B	Foliated hornblende gabbro
78KG127	Foliated hornblende gabbro
78KG128	Foliated hornblende gabbro
78KG130	Lherzolite
78KG131	Gabbro
78KG132	Gabbro
78KG175	Wehrlite
78KG176	Wehrlite
78KG177	Mafic dike
78KG178	Wehrlite
78KG180	Two-pyroxene gabbro
78KG181	Olivine-bronzite cumulate
78KG182	Dunite
78KG183	Foliated hornblende gabbro
78KG184	Foliated hornblende gabbro
78KG185	Olivine-bronzite cumulate
78KG186	Foliated hornblende gabbro
78KG187	Metamorphosed-olivine clinopyroxenite
78KG188	Olivine-pyroxene heteradcumulate
78KG189	Olivine-pyroxene heteradcumulate
78KG190	Serpentinite
78KG191	Foliated hornblende gabbro
78KG192	Hornblende gabbro
78KG193	Altered olivine-bronzite cumulate
78KG194	Olivine-pyroxene heteradcumulate
78KG195	Olivine clinopyroxenite
78KG197	Mafic dike
78KG198	Olivine clinopyroxenite
78KG199	Olivine clinopyroxenite
78KG201	Olivine-pyroxene heteradcumulate

Sample number	Rock name
78KG210	Foliated hornblende gabbro
78KG211	Foliated hornblende gabbro

TINCUP PEAK AREA
SAMPLE LOCALITY MAP